



Methane in Zackenberg Valley, NE Greenland: Multidecadal growing season fluxes of a high Arctic tundra

Johan H. Scheller^{1,2}, Mikhail Mastepanov^{1,3}, Hanne H. Christiansen², Torben R. Christensen¹

¹Department of Bioscience, Arctic Research Centre Aarhus University, Roskilde, Denmark

5 ²Arctic Geology Department, The University Centre in Svalbard, Longyearbyen, Norway

³Oulanka research station, University of Oulu, Finland

Correspondence to: Johan H. Scheller (jscheller@bios.au.dk)

10 **Abstract.** The carbon balance of high-latitude terrestrial ecosystems plays an essential role in the atmospheric concentration of trace gases, including carbon dioxide (CO₂) and methane (CH₄). Increasing levels of atmospheric methane have contributed to ~20 % of the observed global warming since the pre-industrial era. Rising temperatures in the Arctic are expected to promote the release of methane from Arctic ecosystems. Still, existing methane flux data collection efforts are sparse and highly scattered, and further attempts to assess the landscape fluxes over multiple years are needed.

15 Here we use multiyear monitoring from automated flux chambers located on the fringe of a fen area in the center of Zackenberg Valley, northeast Greenland, from July and August (2006–2019). Direct measurements of methane fluxes showed high variability, with mean July–August fluxes ranging from 0.26 to 3.41 mg CH₄ m⁻² h⁻¹. Methane fluxes based on manual chamber measurements are available from campaigns in 1997, 1999–2000, and in shorter periods from 2007–2013 and have been summarized in several published studies. Fluxes from the multiyear monitoring were combined with fluxes from the most common vegetation types, measured in 2007, and a detailed vegetation cover map to assess the methane flux on a landscape-scale and its variability over time.

20 July–August landscape fluxes, estimated in the current study for the 2006–2019 period, were low compared to previous estimations. For the full study area covering the valley floor, the net methane source during these months was estimated as 0.06 to 0.83 mg CH₄ m⁻² h⁻¹ and as 0.26 to 3.45 mg CH₄ m⁻² h⁻¹ for the central fen-rich areas.

25 A 2017–2018 erosion event indicates that some fen and grassland areas along the river in the center of the valley are becoming unstable following pronounced fluvial erosion and a prolonged period of permafrost warming. Although such physical disturbance in the landscape can disrupt the current ecosystem–atmosphere flux patterns, even pronounced future erosion along the river is unlikely to impact methane fluxes at a landscape-scale significantly. Instead, projected changes in future climate in the valley play a more critical role. The results show that multiyear landscape methane fluxes are highly variable at a landscape-scale and stress the need for long-term spatially distributed measurements in the Arctic.

35 1 Introduction

For decades, tundra ecosystems have been subject to attention concerning changing climate. The Arctic is known to be particularly prone to increasing temperatures, and considerable changes to ecosystems at high latitudes were to be expected (IPCC, 1990). Further, high latitude wetlands have, for a long time, been recognized as a significant contributor to the global atmospheric budget of methane (CH₄). In the first global budget, the wetland source was estimated at 130 to 260 Tg y⁻¹ of a total atmospheric burden of 529 to 825 Tg y⁻¹ (Ehhalt, 1974). This term and the overall atmospheric budget have changed remarkably little during nearly 40 50 years of research, with a more recent estimate ranging from 140 to 280 Tg y⁻¹ (Christensen, 2014). It still forms the background for the concern that with Arctic ecosystems warming, including the wetland source



regions, increasing emissions can start a positive feedback in the climate system. In addition to Arctic
45 warming, landscape changes such as permafrost thaw affecting tundra ecosystems and lake formations have
been identified as possible hotspots for increased emissions (Schuur et al., 2015; Walter Anthony et al., 2018).
Also, coastal and further offshore marine sources are subject to possible changed emissions in the Arctic
(Shakhova et al., 2014; Thornton et al., 2020) but these are not dealt with here. Overall, these concerns led to
early and still continuing efforts at quantifying more closely the Arctic natural emissions and their sensitivity
50 and dynamics in relation to climate change.

Studies of tundra methane emissions in several parts of the Arctic were initiated between the 1970s and 1990s
(Svensson and Rosswall, 1984; Whalen and Reeburgh, 1988; Morrissey and Livingston, 1992; Christensen,
1993). The Zackenberg Valley in northeast Greenland was one of the first high Arctic sites to be added to the
circumpolar map of methane flux studies in 1997 (Christensen et al., 2000) after the start of the Zackenberg
55 Ecological Research Operations (ZERO) in 1995 (Meltofte et al., 2008). Since then, the valley has seen
several different methane flux studies, and methane monitoring became part of the Greenland Ecosystem
Monitoring (GEM) program in 2007 (Mastepanov et al., 2013). With numerous short-term research projects,
the monitoring has led to the availability of a unique, large number of years with observations of fluxes
compared to any other location in the Arctic.

60 Here we compile all methane flux studies conducted so far in the valley with the objectives to 1) review the
combined information from these studies on temporal and spatial variability of methane fluxes in a composite
high Arctic landscape and 2) assess the sensitivity of the measured fluxes as they respond to climate warming
or local changes. The large number of studies and multiple years of observations provide a unique opportunity
to disentangle the effect of different processes and quantify their relative influence on the fluxes at the
65 landscape-scale. These processes can broadly be grouped as 1) climate variability and the projections for a
gradual warming, 2) increased erosion of vegetated surfaces.

The challenge is to quantify the sensitivity of the landscape fluxes to these factors individually to allow for a
quantitative analysis of how the factors combine and compare in terms of sensitivity to established climate
warming scenarios.

70 To conduct this study, we use a combination of published data and new measurements of methane fluxes from
a recently eroded gully near the Zackenberg Research Station and its immediate surroundings.

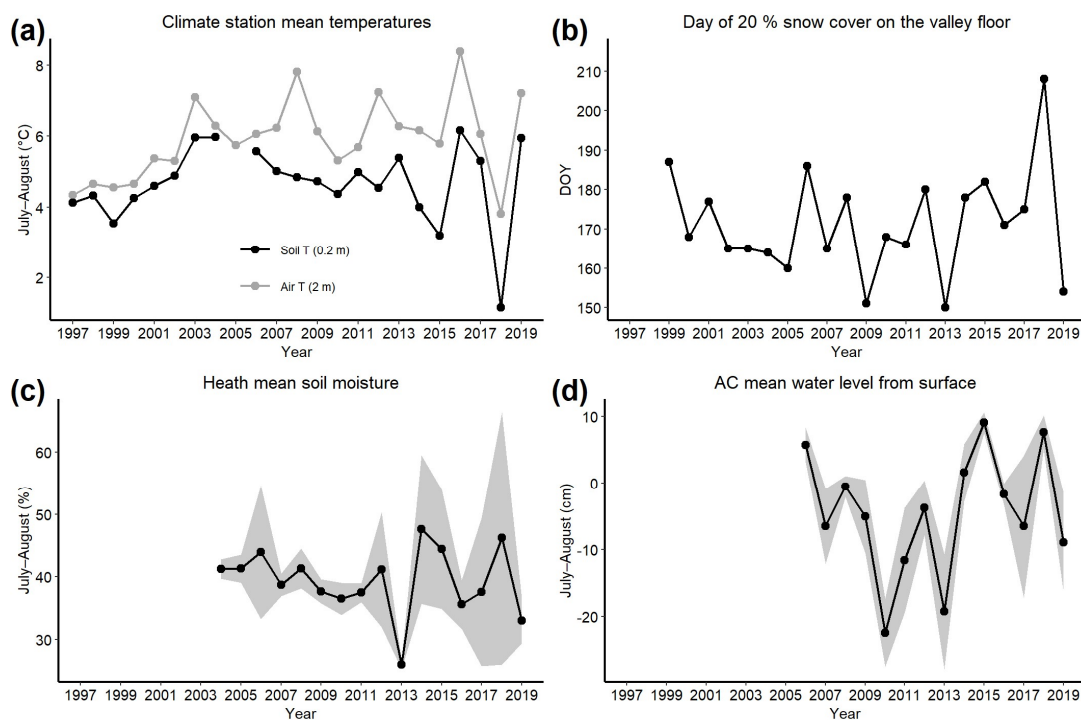
2 Materials and methods

2.1 Site description

Zackenberg Valley is located at 74.47° N, 20.55° W, between 0 to 200 m above sea level (m.a.s.l.) in northeast
75 Greenland. The climate of Zackenberg Valley is high Arctic (Meltofte and Rasch, 2008), with an annual mean



air temperature of $-9.0\text{ }^{\circ}\text{C}$, which increased by $0.06\text{ }^{\circ}\text{C year}^{-1}$ in the 1996–2014 period (Abermann et al., 2017). The warmest month is July, with a mean temperature of $6.3\text{ }^{\circ}\text{C}$ (1997–2014) (Pedersen et al., 2016), and freezing temperatures rarely occurring during the 4–6 weeks of high summer (Hansen et al., 2008). Annual precipitation is measured from 1 September to 31 August and ranged from 222 to 547 mm water equivalent, with a mean of 80 367 mm (1996–2014). The timing of 80 % snowmelt at the valley floor varies from 30 May (DOY 150) to 6 July (DOY 187) between 1999 and 2014 (Pedersen et al., 2016). Continuous permafrost underlies the valley (Christiansen et al., 2008), and the active layer (AL) reaches a maximum depth of 0.58 to 0.85 m, increasing at a rate of 0.74 cm year^{-1} (1996–2019) at the ZEROCALM-1 site (Christensen et al., 2020a) near the climate station at the valley floor. Figure 1a shows the development of July–August soil and air temperatures since 1997 85 at 0.2 m depth and 2 m height measured at the climate station. The timing of snowmelt in the study area (Fig. 1b) varies significantly between years. During July and August, there is so far no clear trend toward drier or wetter conditions for both the heath areas (Fig. 1c) and the fens at the automated flux chambers (AC) site (Fig. 1d) from the mid-2000s and forward.



90

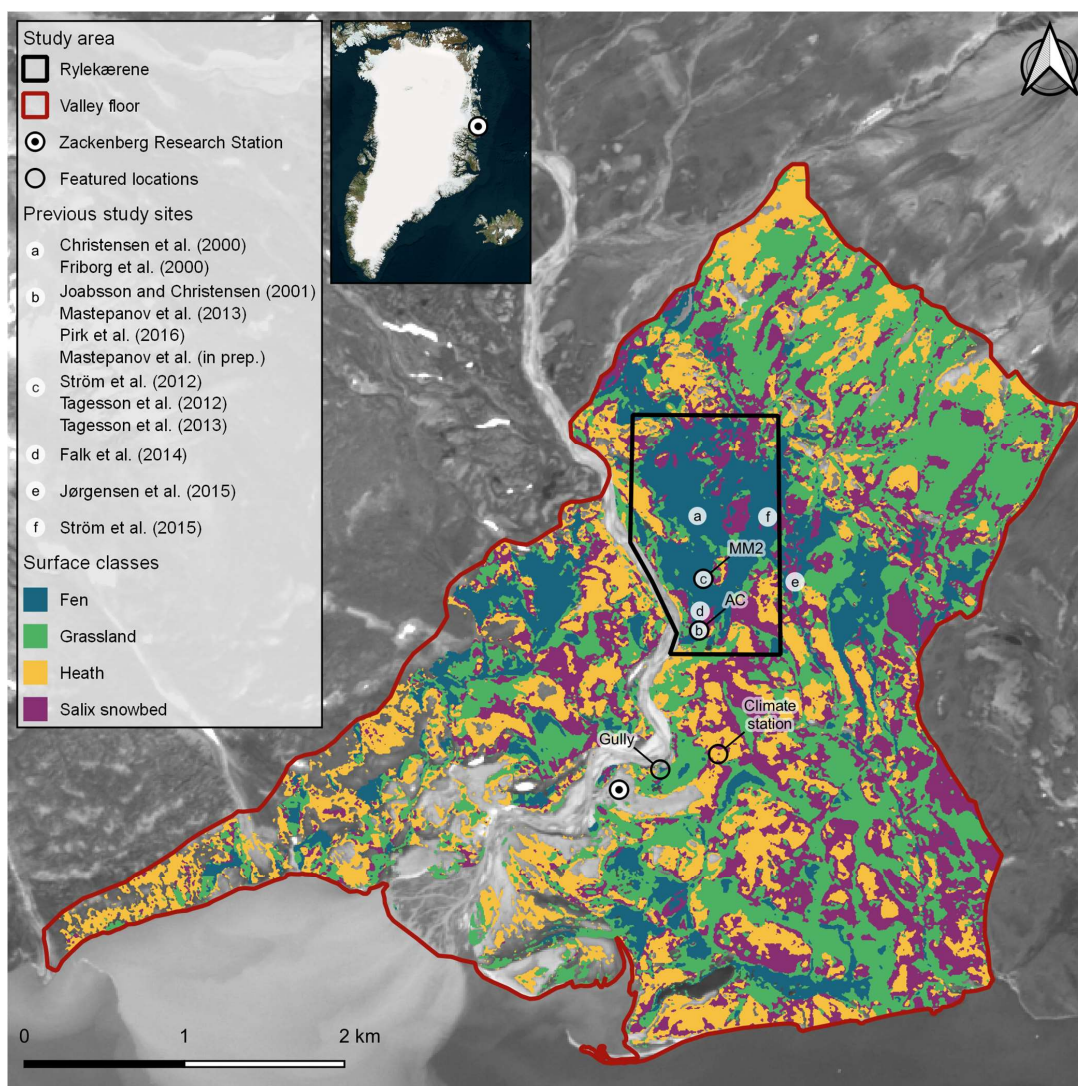
Figure 1: (a) July–August mean temperatures measured at the Zackenberg climate station. (b) Timing of 20 % remaining snow cover on the valley floor with 1999–2014 data from Pedersen et al. (2016). (c) July–August mean soil moisture at the Mix-1 heath site in the lower valley with standard deviation (SD) as shading. (d) July–August mean water level relative to the surface measured close to chamber 1 at the AC site with SD as shading. Please note the differences in the time axes. Data sources: GEM

95 ClimateBasis and GeoBasis Zackenberg.



The study area in the valley follows the boundaries used in Søgaard et al. (2000). The area covers the core monitoring and research projects area of the GEM program (Zone 1A) below 200 m.a.s.l., covering a total area of ~16 km² on the valley floor (Fig. 2). The vegetated areas consist of continuous and hummocky fens, 100 grasslands, *Salix* snowbeds, and *Cassiope* and *Dryas* heaths. Common species in the fens include *Dupontia psilosantha* and *Eriophorum scheuchzeri*, and graminoids, including *Arctagrostis latifolia*, *Eriophorum triste*, and *Alepecurus alpinus* covers the grassland areas. (Bay, 1998)

A subdivision of the valley study area is Rylekærene, a 1.3 km² patterned wet tundra ecosystem dominated by fen areas and divided by drier patches of heaths and grasslands in the central part of the valley (Tagesson et al., 105 2013). Rylekærene has been a subject of several methane flux studies since the mid-1990s (Fig. 2).





110 **Figure 2:** The study area with dark red and black boundaries showing the valley floor study area and Rylekærene in Zackenberg (74.47° N, 20.55° W) and the approximate location of previous study sites marked with letters. The two gas monitoring sites, AC and MM2, are found at the same places as study sites b and c, marked with black circles. Colored areas show the spatial distribution of the four main surface classes used in this study. Areas not covered by the four classes take up 16.9 % of the valley floor and 3.6 % of Rylekærene. *Data sources: HyMap hyperspectral imaging campaign (7 August 2000), ESA Copernicus Sentinel-2 (Grayscale, 16 July 2019), and © Microsoft 2021.*

The first methane flux measurements in Rylekærene were carried out in 1997 in studies by Christensen et al. (2000) and Friberg et al. (2000) using manual flux chamber measurements and the eddy covariance (EC) method in the center of the fen area (Fig. 2a). In the south end of Rylekærene, less than 600 m south of the EC site, Joabsson and Christensen (2001) measured methane fluxes in 1999–2000 (Fig. 2b). Close to this site, the AC setup has measured methane and CO₂ fluxes along a topographic gradient from a wet fen area and a drier grassland area starting in 2005. The AC site is a part of the GeoBasis subprogram of GEM (Mastepanov et al., 2008; Mastepanov et al., 2013).

120 Tagesson et al. (2012) measured methane and CO₂ fluxes by gradient EC methods at a site in the center of Rylekærene in 2008 and 2009. This site (Fig. 2c) is located ~250 m north of the AC site and was later promoted to a permanent EC CO₂ flux installation for measurements in the GeoBasis subprogram under the MM2 (MicroMet 2) name (Lund et al., 2008–2011; Stiegler et al., 2016).
125 In 2007, methane fluxes of the most common vegetation types were measured at 55 plots in a ~600 m² area in the center of Rylekærene, about 300 m north of the AC site (Tagesson et al., 2013), and 50 to 150 m east of the current location of MM2.

More recently, several studies focused on areas outside the permanent AC and MM2 sites, including Falk et al. (2014) (Fig. 2d) and Jørgensen et al. (2015) (Fig. 2e) towards the eastern border of Rylekærene, and Ström et al. (2015) in between the AC site and MM2 (Fig. 2f).

130 A large dendritically shaped gully formed rapidly during July 2018, most likely triggered by substantial lateral erosion of up to 4.7 m in an outer bend of the river after a glacier lake outburst flood (GLOF) in August 2017 (Tomczyk et al., 2020), right where the gully ends. This gully, previously referred to as ‘thermokarst’, extends from Gadekæret, a small fen area close to Zackenberg Research Station (Christensen et al., 2020b). The gully is up to 1 to 4 m deep, up to 8 m wide, and ~50 m long in the longest flow direction. This process is different from thermokarst and is similar to the active development of a gully in the northern part of Zackenberg Valley in 1999 (Christiansen et al., 2008). The retrogressive branching pattern of the gully most likely occurs along ice-wedges in the area. Meltwater from a large snowpack located in Gadekæret in early 2018 saturated the thawed sediments and thermally eroded the ice-wedges, causing sediment transport from the site and into the
140 river.

The gully was monitored closely during the 2019 field season, but its development had come to a halt. Standing water covered the bottom of the gully during August 2018, and elevated methane concentrations were detected in the area (Christensen et al., 2020b). In 2019, the bottom of the gully had dried out, and methane concentrations were no longer elevated.



145 2.2 Measurements

2.2.1 Fluxes from mobile and automated chambers

Most of the previous studies in the research area were based on mobile flux chambers and stationary automatic chambers, which utilized measured changes in methane concentration over time inside a chamber to estimate surface fluxes. The chamber was sealed off to all sides but the bottom during each measurement, isolating the flux estimates to a specific time and area, analogous to the approach described by, e.g., Crill et al. (1988) and Livingston and Hutchinson (1995). Methods vary between the studies, with differences in gas analyzers, chamber designs, measurement time, replication numbers, sampling frequency, and the length of the study periods. The similarities and differences are summarized in Table 1.

155 **Table 1: Flux chamber measurements in Zackenberg Valley vary in several ways between studies. Please see each study for a detailed description of the methods. Only the data used in this study are included in the table, i.e., unmanipulated and control plots.**

Publication and study year	Gas analysis	Chamber design	Sampling time	Plots	Measurement frequency
Christensen et al. (2000) in 1997	Duplicate syringe sample in two 10 to 15 min intervals. Analysis with a Shimadzu GC14-B gas chromatograph	13 to 30 L, aluminum dark chambers on bases permanently inserted to 10 to 20 cm depth	20 to 30 min	30 plots in five sites	Two times per week
Joabsson and Christensen (2001) in 1999–2000	Duplicate syringe samples were taken at regular intervals. Analysis with a Shimadzu GC14-B gas chromatograph	14 to 22 L, aluminum dark chambers on permanently installed bases (15 cm depth)	NA	Six plots in one site (only control plots)	One to three times per week
Ström et al. (2012) in 2007	LGR DLT200 analyzer	2.2 L, transparent chamber on permanently installed aluminum bases (set-up ¹)	3 min	15	Two to four days interval
Mastepanov et al. (2013) in 2006–2010	LGR DLT100 model 908-0007	~108 L permanently installed transparent, automatic chambers	5 min	Four (2006) Six (2007–2010)	Every hour
Tagesson et al. (2013) in 2007	LGR DLT200 analyzer	10 L, transparent chamber inserted into ~2 cm notches in the ground	3 min	55 plots in seven sites	Two to three times per week
Falk et al. (2014) in 2009–2012	LGR DLT200 analyzer and Gasmeter Dx 40-30 Fourier transform infrared spectrometer	41 L, transparent and dark chambers on bases permanently installed to 15 cm depth	3 to 7 min	15 plots in one site (only unmanipulated plot)	Approximately two times per week
Jørgensen et al. (2015) in 2012	LGR DLT100 analyzer	Volume NA, Transparent and dark chambers on permanent bases inserted to ~10 cm depth	10 min	40 plots in four sites	NA, 280 samples in total during four campaigns
Ström et al. (2015) in 2011–2013	Gasmeter Dx 40-30 Fourier transform infrared spectrometer	41 L, transparent and dark chambers on bases permanently installed to 15 cm depth	3 to 7 min	16 to 20	Approximately two times per week
Pirk et al. (2016b) in 2012 and 2014, Mastepanov et al. (in prep.) in 2011 to 2019	LGR Greenhouse Gas Analyzer model 908-0011	~108 L permanently installed transparent automatic chambers	5 min	10	Every 90 minutes

For the aims of the current study, we analyzed existing data of July–August CH₄ fluxes from manual mobile chamber measurements from 2007, published in Tagesson et al. (2013), and GeoBasis Zackenberg automatic



chamber measurements (2006–2010 published in Mastepanov et al. (2013), and 2011–2019 in Mastepanov et al. (in prep.). Details on the methods are described in these publications. Only parts of the AC flux time series were used in this study; the July–August flux includes the peak of the growing season in the valley, and it matches the timing of most of the previous studies.

165 In addition to this data, we carried out 113 measurements from 23 August 2019 to 1 September 2019 in a grid covering the recent gully (see Fig. 2) and extending toward a small lake in the Gadekæret fen area close to Zackenberg Research Station.

The measurements took place between 9 a.m. and 7 p.m. on 43 plots located 4 to 5 m from each other in the three main surface classes in the area: fen, grassland/barren area, and the recently eroded area. Several flux
170 measurements at each surface class were performed every day.

A metal collar was carefully installed on the ground on each plot; a dark acrylic chamber was placed over the collar for a minimum of five minutes. The footprint of the collar was 0.07 m²; the height from the soil surface to the top of the chamber was recorded for each measurement (ranged from 0.26 m to 0.48 m depending on the surface topography). The chamber was equipped with a fan inside and had a 3 mm vent on the side. A gas
175 analyzer (Ultraportable Greenhouse Gas Analyzer, Los Gatos Research, USA) was connected to the chamber with a pair of 15 m long HDPE tubes and was continuously measuring CH₄ concentration in the chamber headspace at 1 Hz frequency. After each sample, the chamber was ventilated for at least two minutes until the methane concentration was down to ambient concentration.

2.2.2 Hyperspectral classification

180 The hyperspectral remote sensing data were collected on 8 August 2000 by an airborne HyMap campaign (Palmtag et al., 2015). The image data were processed into a 5 m × 5 m resolution land cover map of Zackenberg Valley (Elberling et al., 2008), improving on a manual land cover classification by Bay (1998). Zackenberg River has changed its course since 2000 after multiple GLOF events (Søndergaard et al., 2015; Tomczyk and Ewertowski, 2020), and we adjusted the land cover classification map to fit the extent of the river in a 2014
185 orthomosaic of the entire study area (COWI, 2015).

2.3 Data processing

2.3.1 Measurements from mobile and automated chambers

Data from Tagesson et al. (2013) included seven different surface classes: continuous fen ($n = 154$), hummocky fen ($n = 108$), grassland ($n = 110$), *Salix* (willow) snowbeds ($n = 51$), *Vaccinium* heath ($n = 54$), *Cassiope* heath
190 ($n = 54$), and *Dryas* heath ($n = 54$). The fluxes on the seven land cover classes were further summarized into four general classes. The two fen classes were combined, and so were the three heath classes. In the valley-wide vegetation cover map, hummocky and continuous fen were not separated into different classes, even though mean fluxes differ substantially for these two surface types (see Table 3 in Tagesson et al. (2013)). A weighted



mean flux, taking the different sample sizes for the separate land cover classes into account, was calculated and
195 used for this study.

The fluxes at the AC site were calculated from each automatic chamber measurement, using the same approach
as Mastepanov et al. (2013). The flux time series was separated into two datasets: one representing a long time
series from the fen fringe (chambers 1 to 6). Another time series represents the changes since 2012 in the four
outer chambers, located further out in the fen (chambers 7 to 10). The flux data do not show a diurnal pattern
200 for July and August, so all available data for each chamber were used in those two months. Data from chambers
1 to 6 were first summarized for each chamber as temporal means, highlighting the differences in fluxes from
each of the six inner chambers. July–August data were then further summarized into a single mean methane
flux for each year. In 2006, only four chambers were operating, and no data were available for chambers 4 and
6. The difference is corrected by multiplying the mean of the available 2006 data by a coefficient based on 2007
205 data. This coefficient was found by dividing the mean in chambers 1, 2, 3, and 5 by the mean of all six chambers.
Multiyear methane flux measurements enabled a comparison between years, and the flux estimates from
chambers 1 to 6 at the fen fringe are used for a spatial upscaling of methane fluxes using R (R Core Team,
2020). The July–August mean flux for each year in the 2006–2019 period ($Flux_{AC,year}$) was divided with the
2007 July–August mean flux ($Flux_{AC,2007}$ in Eq. 1), making it comparable to the timing of the mobile chamber
210 measurements from Tagesson et al. (2013). This calculation gave a number less than 1 in years with
comparatively low flux and more than 1 in years with relatively high flux. It is used below as a coefficient
($AC_{coefficient,year}$) for estimating the landscape fluxes in the 14-year time series.

$$AC_{coefficient,year} = \frac{Flux_{AC,year}}{Flux_{AC,2007}} \quad (1)$$

215 2.3.2 Land-cover classes

The four combined surface classes represent most of the study areas (Rylekærene and the valley floor, Table 1).
In Eq. (2), the areal coverage ($Area_{class}$) of the surface classes was calculated using QGIS v. 3.10.0 (QGIS.org,
2020). The flux for 2007 ($Flux_{class,2007}$) and the area-weighted flux were calculated for the two study areas, the
valley floor and Rylekærene ($Area_{total}$). This approach assumes no fluxes of methane in the remaining parts of
220 the study areas, including delta, river, and primarily barren areas (Fig. 2). The area-weighted landscape flux
($Flux_{area\ weighted, 2007}$) calculation is shown in Eq. (2), and classes include fen, grassland, *Salix* snowbeds, and
heath.

$$Flux_{area\ weighted, 2007} = \frac{\sum(Flux_{class,2007} \times Area_{class})}{Area_{total}} \quad (2)$$



225 2.3.3 Combining data into a landscape flux time series

An area-weighted landscape methane flux for each measurement year ($Flux_{year}$) is estimated by combining Eq. (1) and Eq. (2) in Eq. (3). The area-weighted mean landscape flux in 2007 ($Flux_{area\ weighted, 2007}$) is multiplied with the coefficient representing the relative changes in mean flux relative to 2007 ($AC_{coefficient, year}$), creating a time series of July–August fluxes from 2006 to 2019.

230

$$Flux_{year} = Flux_{area\ weighted, 2007} \times AC_{coefficient, year} \quad (3)$$

2.3.4 Fluxes in the gully area

In the recently eroded gully area, the fluxes in 2019 were calculated using the linear flux model (Pirk et al., 2016a). Of the 113 measurements, 102 had a significant ($p < 0.05$) regression slope. The remaining 11
235 measurements were found on both the grassland/barren areas and on recently eroded surfaces. They showed an increase in concentration over time close to zero, and they are interpreted as areas with a zero flux. The 11 measurements are included in the calculation of the mean flux of the recently eroded surfaces in the gully.

The mean flux and the standard error (SE) for all measurements were calculated by calculating the mean flux for repeated measurements for each plot. Further averaging for their respective surface class (recent erosion,
240 barren/grassland, fen) was done afterward, showing how fluxes can change in an area after an erosion event.

2.3.5 Valley flux and future impacts on methane emissions with increasing erosion activity

Recent active riverbank erosion in Zackenberg Valley raises the question of how the methane flux on a valley-scale will change with increasing erosion in the future, and the sensitivity to such changes is explored below. The valley flux for the late 21st century is estimated based on Geng et al. (2019), Geng (personal communication,
245 24 April 2020), and the mean valley flux results from 2008–2015. The relative change in methane flux from present-day conditions to 2081–2100 conditions under the Representative Concentration Pathway 8.5 (RCP8.5) forced with the ECHAM5 general circulation model is estimated to increase by a factor of 2.43.

The mean July–August methane flux for the valley is here assumed to change linearly to a 2.43 times higher flux between 2016–2100, which allows us to include an intermediate time-step (2041–2060). Over the same
250 period, further erosion in the valley is simulated to assess the importance of surface erosion in Zackenberg on methane relative to changes in fluxes increasing temperatures. Multiple sites in Zackenberg Valley are subject to active erosion, and several of these sites are found along the Zackenberg River (Tomczyk et al., 2020). Here we hypothesize large-scale erosion along the river in the 21st century to improve our understanding of its importance on valley-wide methane fluxes, although an increase of eroded surface areas of this magnitude is
255 unlikely.

The impacts on methane are estimated from a linear development in eroded surfaces from 0 m to 25 m and from 0 m to 100 m on each side of the Zackenberg River. The development change areas that act as sinks or sources

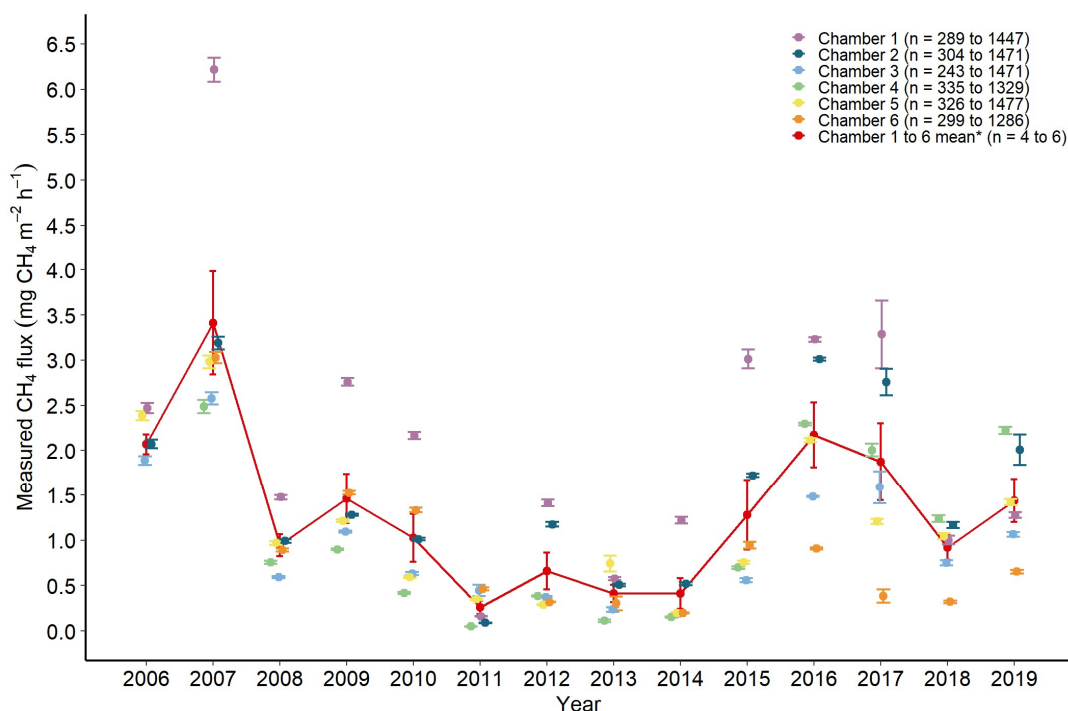


of methane into eroded areas, using the mean flux measured on the recently eroded surfaces in the gully in 2019. The Zackenberg River was digitized to its extent in August 2014, when the valley was mapped in high detail (COWI, 2015). Eighty-five buffer zones were created on each side of the river, each representing one year. These buffer zones had a total width of 25 m and 100 m. The land cover types in each buffer zone were progressively eroded for the sensitivity study, and the associated change in methane flux was subtracted from the mean valley methane flux.

3 Results

3.1 Temporal variability in flux

From 1 July to 31 August, methane fluxes measured at six chambers available for the entire 2006–2019 period at the AC site show spatial and temporal variability both within years and between years (Fig. 3). Results for the entire growing season have earlier been published for 2006–2010, where fluctuations and patterns within years are analyzed, focusing on the variations in the mean flux of six chambers (Mastepanov et al., 2013). Treating all six chambers as replicates reveal high temporal variability for the area (red points and line in Fig. 3). The highest July–August mean flux (\pm SE) for all six chambers was $3.41 \pm 0.57 \text{ mg m}^{-2} \text{ h}^{-1}$ in 2007. The lowest mean flux of all six chambers was $0.26 \pm 0.07 \text{ mg m}^{-2} \text{ h}^{-1}$ in 2011, and the mean flux for all chambers for all 14 seasons was $1.27 \pm 0.01 \text{ mg m}^{-2} \text{ h}^{-1}$. Error bars (SE) around the mean of chambers 1 to 6 express the spatial variability between chambers for each year. The spatial variability was smallest in 2011 and the highest in 2007. Figure 3 shows no clear trend in July–August mean methane flux over the 14 years. Not shown here are the individual mean fluxes for the four chambers operating further out in the fen since 2012. These chambers, named chambers 7 to 10, generally show higher fluxes than those measured at chamber 1 in Mastepanov et al. (2013) and Mastepanov et al. (in prep.).



280

Figure 3: Time series of July–August AC methane measurements from 2006–2019. Chamber 1 through chamber 6 show the temporal mean of fluxes and error bars show the SE of the temporal variability. The red dots and lines show the spatial mean of the fluxes in chambers 1 to 6 with error bars displaying the SE between chambers. The range of observations (n), as the quantity changes through time. *The SE for Chamber 1 to 6 mean is calculated from the mean of each chamber, which explains the low number of observations. Data source: GEM GeoBasis Zackenberg.

285

3.2 Surface cover

The area of four surface classes of the valley floor and the fen-dominated Rylekærene was calculated based on HyMap data from August 2000. The surface classes used in this study are a subset of the HyMap dataset, combining heath classes and excluding ‘Other’ surface classes. This class includes barren areas, lakes, and rivers. The four surface classes cover most of the valley (Fig. 2), with the notable exemptions of the Zackenberg River system and the landing strip. The four surface classes cover 83.1 % of the valley study area and 96.4 % of the Rylekærene study area, where most methane studies in the valley were carried out (Fig. 2).

290

Table 2 shows the coverage of each surface class compared to the valley floor and Rylekærene areas in both absolute and relative terms. The fen surface class takes up 12.1 % of the valley floor while accounting for 50.4 % of the Rylekærene study area. Grassland and heath areas are common (28.5 % and 21.8 %) in the valley floor area while being relatively less important in Rylekærene. Salix snowbeds take up 20.7 % and 21.1 % in the two

295



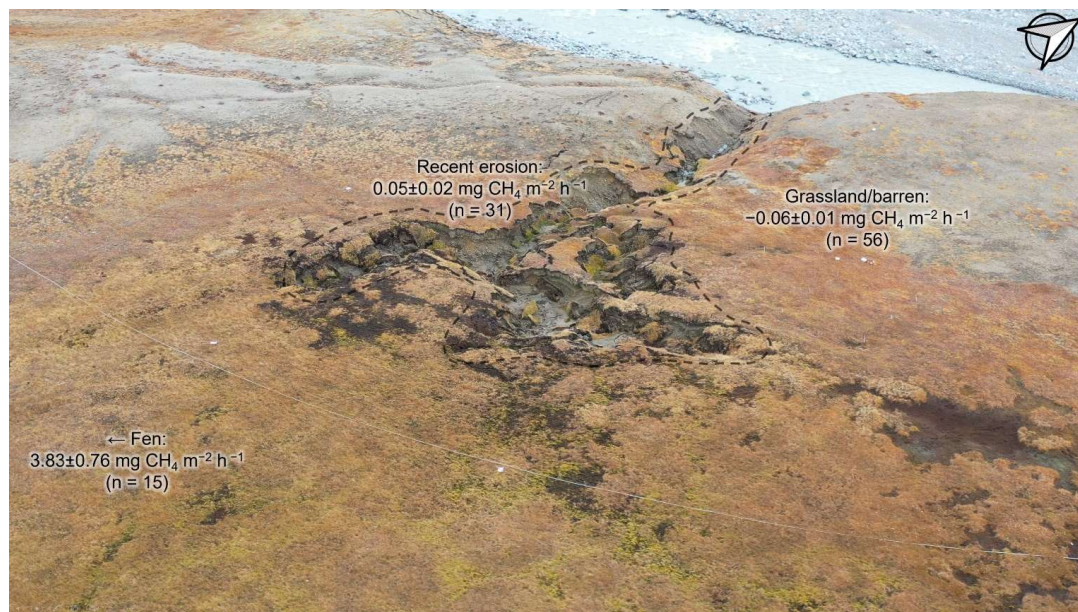
study areas. The relative composition of the two study areas is used for estimating the area-weighted methane landscape flux for the time series.

300 **Table 2: Absolute and relative area distribution for the four main surface cover classes in the two study areas from HyMAP classification updated to the Zackenberg River extent in 2014.**

Surface class	Valley floor in m ² (% of the area)	Rylekarene in m ² (% of the area)
Fen	1,916,658 (12.1 %)	641,368 (50.4 %)
Grassland	4,536,727 (28.5 %)	177,805 (14.0 %)
Heath	3,465,133 (21.8 %)	139,167 (10.9 %)
<i>Salix</i> snowbeds	3,294,996 (20.7 %)	267,819 (21.1 %)
Other (e.g. barren & water)	2,691,489 (16.9 %)	45,144 (3.6 %)
Total	15,905,003 (100 %)	1,271,303 (100 %)

3.3 Gully methane fluxes

The methane flux at the exposed, eroded surfaces of the gully was different from the flux on the nearby, 305 undisturbed surfaces (Fig. 4). The late growing season mean methane flux of the recently eroded surfaces in the gully in 2019 was $0.05 \pm 0.02 \text{ mg m}^{-2} \text{ h}^{-1}$, with both positive and negative fluxes. The Grassland/barren surface cover in areas not disturbed by erosion shows a negative methane flux of $-0.06 \pm 0.01 \text{ mg m}^{-2} \text{ h}^{-1}$. The mean methane flux in the fen was $3.83 \pm 0.76 \text{ mg m}^{-2} \text{ h}^{-1}$, more than 75 times higher than the mean flux in the gully. Methane emissions generally increased closer to the open water body of the nearby fen. The emergence of the 310 gully marked a transition from a small methane sink to a small source for this area. The source followed an initial substantial episodic release of methane stored in exposed ice in the year when the gully appeared (Christensen et al., 2020b).



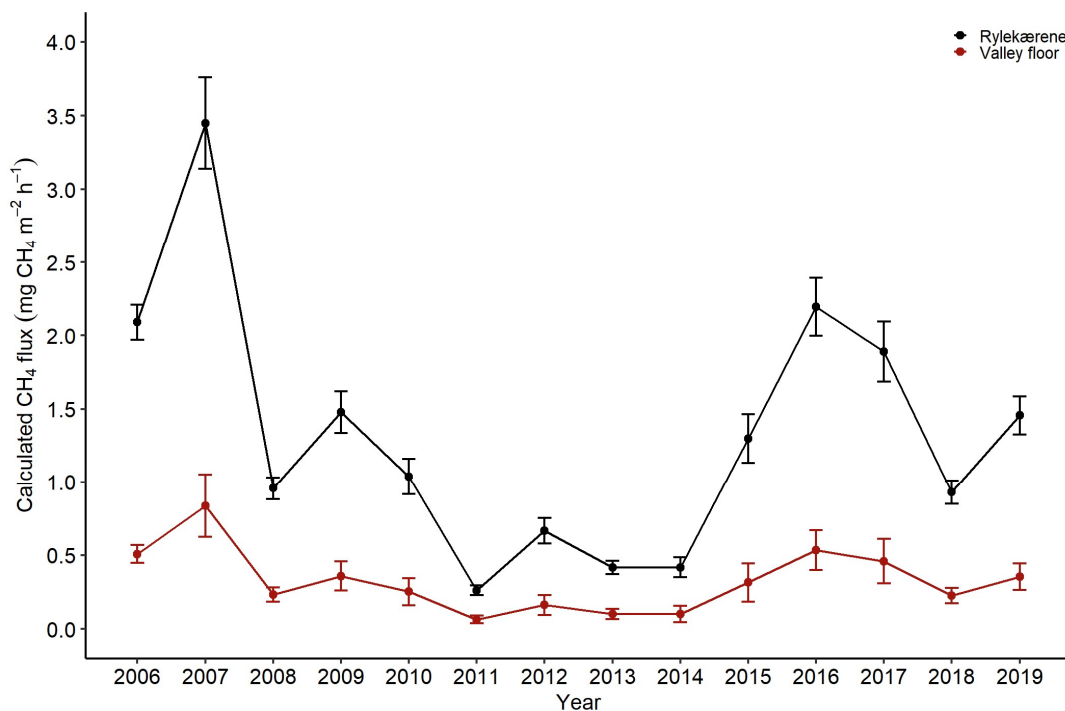


315 **Figure 4: The gully and fen area near the Zackenberg Research Station. Numbers show the measured methane fluxes on different surface types between 23 August and 1 September 2019, when this image was captured. The dashed black line indicates the approximate boundaries of the gully, which is ~50 m long and ~25 m at its widest. The nearby fen is located outside the image, ~30 m south of the gully.**

3.4 Estimation of an integrated flux of methane in Zackenberg Valley

320 The July–August landscape flux of methane showed large interannual variability over the valley floor and Rylekærene study areas over the 14 years, 2006–2019. We observed no apparent trends (*Pearson's* $r = -0.22$, $p = 0.44$) over the entire period (Fig. 5). The mean flux for the 2006–2019 period was $1.32 \pm 0.14 \text{ mg m}^{-2} \text{ h}^{-1}$ and $0.32 \pm 0.05 \text{ mg m}^{-2} \text{ h}^{-1}$ for the Rylekærene study area and the valley floor. The methane fluxes ranged from $0.26 \pm 0.03 \text{ mg m}^{-2} \text{ h}^{-1}$ in 2011 to $3.45 \pm 0.31 \text{ mg m}^{-2} \text{ h}^{-1}$ in 2007 in Rylekærene and from $0.06 \pm 0.03 \text{ mg m}^{-2} \text{ h}^{-1}$ to $0.83 \pm 0.21 \text{ mg m}^{-2} \text{ h}^{-1}$ for the valley floor. The two study areas were net sources of methane throughout

325 h⁻¹ to $0.83 \pm 0.21 \text{ mg m}^{-2} \text{ h}^{-1}$ for the valley floor. The two study areas were net sources of methane throughout the period, although the source size changed significantly between years.



330 **Figure 5: The calculated area-integrated July–August methane fluxes and SE for Rylekærene and the valley floor from 2006–2019.**



3.5 Methane emissions from the valley in a changing climate

The mean valley methane flux for July–August is shown for 2008–2015, 2041–2060, and 2081–2100 (Fig. 6). For the two future periods, the mean fluxes are depicted as changed in an RCP8.5 scenario together with the sensitivity to surface erosion changes. The mean valley flux, excluding erosion, was $0.2 \text{ mg m}^{-2} \text{ h}^{-1}$ for 2008–2015, $0.32 \text{ mg m}^{-2} \text{ h}^{-1}$ for 2041–2060, and $0.45 \text{ mg m}^{-2} \text{ h}^{-1}$ for 2081–2100. The valley methane flux decreases when the eroded surfaces increase in areas with grasslands and fens. The conversion of areas with a methane uptake (Heath areas and *Salix* snowbeds) increases the valley flux. The net effect of the contributions to the mean valley flux from the four surface types is negative, reducing the mean valley flux. The net reduction from erosion is -0.3% and -1.6% in the 2041–2060 period, increasing to a mean net reduction of -0.7% and -7.8% between 2081–2100.

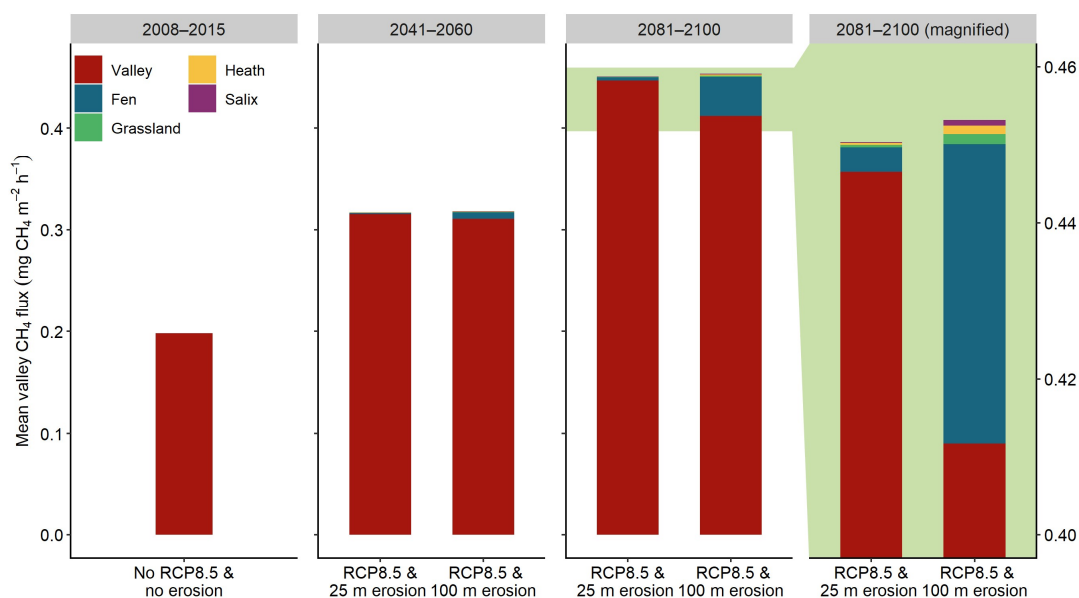


Figure 6: In the RCP8.5 scenario, the mean July–August valley methane flux increase over time, summarized here in two future periods, 2041–2060 and 2081–2100. Increases in flux from rising temperatures are partly offset by erosion in the sensitivity study. The increasing erosion of the four surface classes could change the mean flux of methane in the valley over time. While erosion of grasslands and fens act as relative methane sinks, some of that sink is counterbalanced by a relative source from the loss of *Salix* snowbeds and Heath areas.



4 Discussion

4.1 Methane studies in Zackenberg Valley

Methane flux has been the subject of several measurement campaigns in Zackenberg Valley since 1997. The length of these campaigns, their onset compared to the beginning of the growing season, the sampling area, and strategy varied between studies. Figure 7 shows a timeline of methane flux campaigns from published studies and data from the annually updated GEM database. The approximate locations of the measurement sites are shown in Fig. 2, and a summary of the mean methane fluxes is shown in Fig. 8. With the exemption of Tagesson et al. (2012), which reported mean fluxes specifically for the 2008–2009 growing seasons, the following mean values cover the length of the whole measurement period.

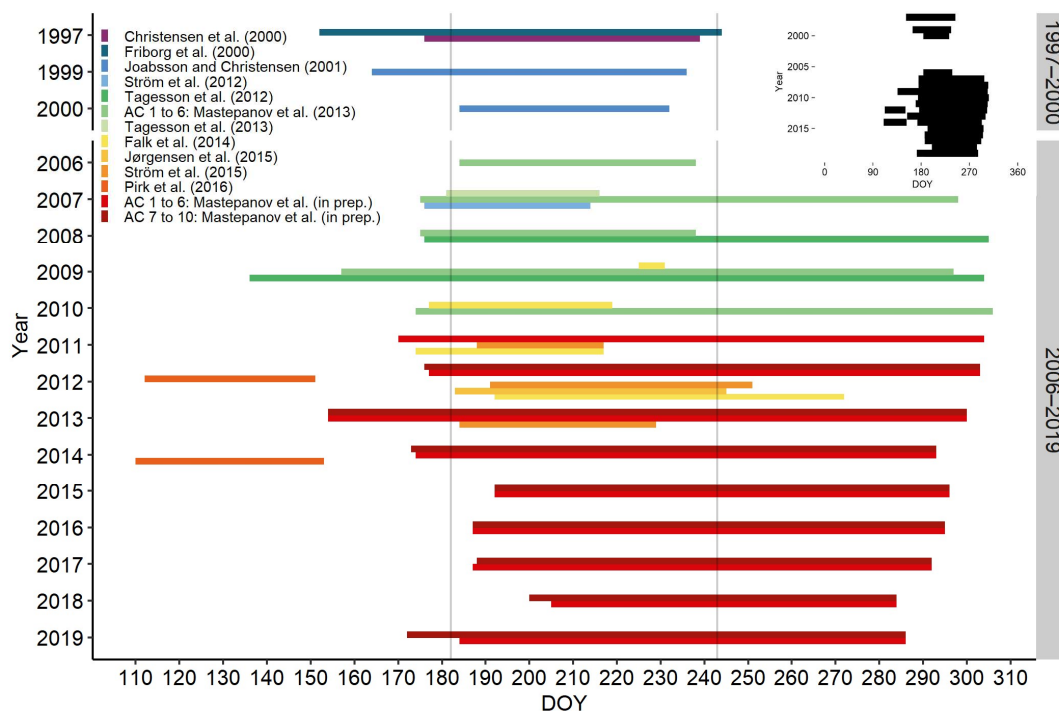
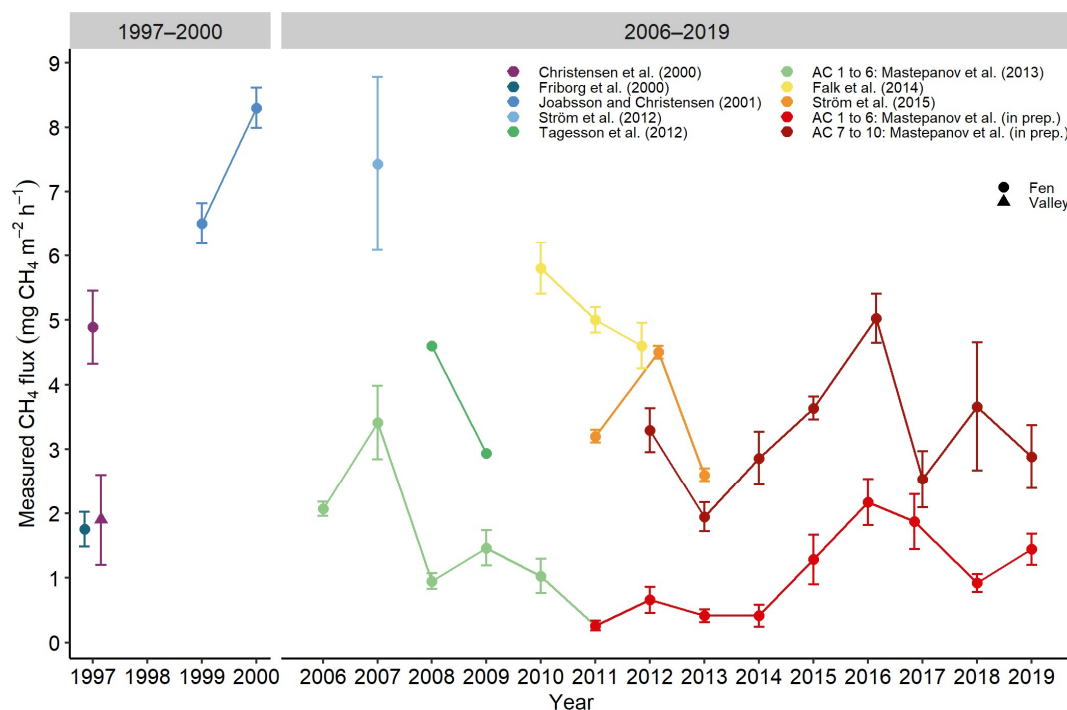


Figure 7: Timeline of methane fluxes measured during the growing season (1 July–31 August for AC) in Zackenberg Valley, covering both fen areas and area-integrated fluxes for Rylekærene and the valley floor. Colors show different publications, and marker shapes indicate the location. Please note that the years 2001–2005 are left out, as no published studies focusing on methane fluxes in undisturbed areas were made in this period. Also, note that points may be shifted slightly along the year axis to avoid overplotting.

Using a distributed manual chamber approach, Christensen et al. (2000) measured a flux for an intensive study area, a part of Rylekærene, of 4.9 ± 0.6 (mean \pm SE) $\text{mg m}^{-2} \text{h}^{-1}$ in 1997. Friborg et al. (2000), using the EC method, found a methane flux for approximately the same area in the same year of 1.75 ± 0.27 $\text{mg m}^{-2} \text{h}^{-1}$, i.e., less than half the mean flux in Christensen et al. (2000). This difference was attributed to a higher proportion



of drier areas in the fetch of the eddy tower. Using the Zackenberg vegetation map of Bay (1998), Christensen et al. (2000) used the flux measured at each of the surface cover types to calculate a mean valley flux of $1.9 \pm 0.7 \text{ mg m}^{-2} \text{ h}^{-1}$. Joabsson and Christensen (2001) measured methane flux at control plots for a plant treatment study in 1999 and 2000, near the southern boundary of Rylekærerne. The mean methane flux was $6.5 \pm 0.32 \text{ mg m}^{-2} \text{ h}^{-1}$ in 1999 and $8.3 \pm 0.31 \text{ mg m}^{-2} \text{ h}^{-1}$ in 2000. Control plot data from a comparable experimental manipulation by Ström et al. (2012) gave a mean of $7.43 \pm 1.35 \text{ mg m}^{-2} \text{ h}^{-1}$ near the current MM2 site. Mastepanov et al. (2013) published the first multiyear methane flux time series, covering the growing season four years from 2006–2010 at the AC site. These measurements continued in 2011–2019 (Mastepanov et al., in prep.). Data from the AC time series were reanalyzed for the 2006–2019 period, only taking fluxes in July–August into account. The mean of all measurements in the six chambers that have been operational through this entire period was $1.27 \pm 0.01 \text{ mg m}^{-2} \text{ h}^{-1}$. Four chambers were added in 2012, which extended the chamber measurements further out into the fen. These four chambers showed generally higher methane fluxes, ranging from $1.95 \pm 0.23 \text{ mg m}^{-2} \text{ h}^{-1}$ in 2013 to $5.03 \pm 0.38 \text{ mg m}^{-2} \text{ h}^{-1}$ in 2016, and a mean flux of $3.36 \pm 0.02 \text{ mg m}^{-2} \text{ h}^{-1}$ for the 2012–2019.



380

Figure 8: Timeline of methane fluxes measured during the growing season (1 July–31 August for AC) in Zackenberg Valley, covering both fen areas and area-integrated fluxes for Rylekærerne and the valley floor. Colors show different publications, and marker shapes indicate the location. Please note that the years 2001–2005 are left out, as no published studies focusing on methane fluxes in undisturbed areas were made in this period. Also, note that points may be shifted slightly along the year axis to avoid overplotting.

385



Tagesson et al. (2012) estimated the integrated methane flux in Rylekærene at the current MM2 site (Fig. 2) using the gradient flux method for the growing season in 2008 and 2009. They found a flux of $4.6 \text{ mg m}^{-2} \text{ h}^{-1}$ and $2.94 \text{ mg m}^{-2} \text{ h}^{-1}$, with alternative error reporting.

Based on measurements in the growing seasons 2010–2012, Falk et al. (2014) reported a mean methane flux of
390 $5.8 \pm 0.4 \text{ mg m}^{-2} \text{ h}^{-1}$, $5.0 \pm 0.2 \text{ mg m}^{-2} \text{ h}^{-1}$, and $4.6 \pm 0.35 \text{ mg m}^{-2} \text{ h}^{-1}$, respectively, for 2010, 2011, and 2012 in untreated plots in Rylekærene. In this same northwestern part of Rylekærene Ström et al. (2015) used mobile flux chambers at multiple (16+) untreated plots and measured during three field campaigns in 2011, 2012, and 2013 a mean methane flux of $3.2 \pm 0.1 \text{ mg m}^{-2} \text{ h}^{-1}$, $4.5 \pm 0.1 \text{ mg m}^{-2} \text{ h}^{-1}$, and $2.6 \pm 0.1 \text{ mg m}^{-2} \text{ h}^{-1}$, respectively.

395 Three studies are omitted in Fig. 8: Pirk et al. (2016b) studied the methane fluxes in the fen areas near the AC site under snow-covered conditions before the growing season in 2012 and 2014. Jørgensen et al. (2015) added flux measurements from 2012 covering only dry tundra sites acting as a methane sink (*Dryas* heath, abrasion plateau, and fell field) and moist tundra (*Salix* snowbeds and *Cassiope* heath). These findings confirmed the atmospheric sink of the dry tundra heath, first reported by Christensen et al. (2000). Tagesson et al. (2013),
400 which provide data for the landscape fluxes in this study, used a modeling approach for calculating a flux time series in Rylekærene covering 1997, 2000, 2002, and 2007–2010. Their study was based on both in situ flux measurements and modeling using environmental parameters and satellite imagery, meaning their results are not directly comparable to the in situ measurements shown in Fig. 8.

405 The studies show large differences in methane flux within the same fen ecosystem. Local spatial variability, interannual differences may explain these differences, and possibly also by differences in methods.

Spatial variability in methane flux can be pronounced in tundra ecosystems with complex microtopography (Olefeldt et al., 2013) and differ significantly even at a meter-scale (Fig. 3). Methane fluxes vary with local differences in substrate, water-table depth, grazing, and vegetation composition and productivity, each of which
410 can either increase or limit the methane flux. Several of these interactions have been studied in Zackenberg Valley: increased substrate availability, mainly acetate, contributes to higher methane fluxes as shown by, e.g., Ström et al. (2003), while a low water table limits methane fluxes (Tagesson et al. (2013). Grazing can either increase (Falk et al., 2015) or decrease (Falk et al., 2014) the methane flux, depending on the vegetation cover. Vegetation composition and primary productivity are strong drivers of methane fluxes (Joabsson and
415 Christensen, 2001; Ström et al., 2012; Ström et al., 2015).

Temporal variability in methane fluxes can be caused by differences in environmental parameters, both within a growing season and from one year to another. Soil temperature was found to explain less variability than species composition and primary productivity (Christensen et al., 2000; Ström et al., 2012), while soil temperatures showed a high correlation with methane flux within most individual years (Mastepanov et al.,
420 2013). Late-lying snow delays the beginning of the growing season (Grøndahl et al., 2008), which controls several of the parameters mentioned above. Only a few studies in Zackenberg Valley were conducted outside the growing season. However, the fall season could substantially impact the annual methane budget, mainly



through emissions associated with the onset of soil freezing (Mastepanov et al., 2008). In contrast, wintertime (November–May) emission may only have a limited impact on the annual methane budget (Pirk et al., 2016b).
425

Our analysis focuses on the mean of the July–August fluxes in the valley, but the automated chambers are running from snowmelt to the end of the field season (Fig. 7). The fixed period matches the timing of the previous studies, and the period showed a good representation of the mean flux of the entire measurement dataset. The first 30 to 40 days after snowmelt have been shown to express the main differences between years
430 (Mastepanov et al., 2013), which is covered by the July–August means to a large extent.

4.2 Landscape methane fluxes

The AC site is located by the outlet of the Rylekærene fen. The substantial flow of water through the area affects the water level, particularly at the innermost six chambers, which are located along the slight topographic gradient at the fen fringe. The changing water level may control the methane flux and explain its high variability
435 2006–2019, but neither the water levels, the air, nor soil temperatures correlate significantly (p -value threshold of 0.05) with methane when analyzing the interannual variability for July–August mean values. Over the 14 years, p -values range from 0.29 to 0.56. The lack of correlation over the time series illustrates a complex interaction between methane and environmental conditions when analyzed on a decadal scale. Figure 8 shows the methane flux of previous studies, which have mainly focused on wetter parts of the fen where the flux is
440 high. The flux appears to vary relatively less over time further out in the fen, as the soil moisture conditions change less between years than the chambers 1 to 6 at the AC site. One example is the smaller relative variability at chambers 7 to 10. The sizeable interannual variability shown in Fig. 3 could be more common for the smaller, discontinuous fen areas in the valley seen in Fig. 2. These areas are characterized by a less stable inflow of water than Rylekærene, which may therefore cause high interannual variability in the transition zones between
445 different vegetation types.

Vegetation plot measurement on the dominant vegetation classes in 2007 combined with long-term AC site data from 2006–2019 enables the calculation of landscape flux time series for Rylekærene and the valley floor. This approach is more direct than modeling based on physical parameters that have otherwise been shown to correlate
450 well with methane flux for Rylekærene (Tagesson et al., 2013). However, a limitation of the approach is its lack of a dynamic component, which could take spatial differences across the valley into account, e.g., snow cover or changing soil moisture conditions from one year to another, affecting the valley floor and the AC site differently.

Tagesson et al. (2013) found a significant difference in the methane flux in hummocky and continuous fen areas
455 in Rylekærene and treated the two groups separately. These groups were combined in this study to match the existing, valley-wide surface cover classification. Comparing the mean flux in Rylekærene over approximately the same period shows good agreement between the flux estimates in this study and the flux in Tagesson et al.



(2013). Four growing seasons (2007–2010) are common for the two studies, and in three years, the flux estimates of this study lie within the model uncertainty in Tagesson et al. (2013). The one notable exemption is
460 the 2007 mean flux ($3.45 \pm 0.31 \text{ mg m}^{-2} \text{ h}^{-1}$) in this study, and it differs a lot from the $1.6 \pm 1.0 \text{ mg m}^{-2} \text{ h}^{-1}$ modeling result. The difference can be explained with a relatively high flux measured at the AC site in a year without extreme temperature or moisture conditions in the valley (Fig. 1), which are central parameters in the modeling of Tagesson et al. (2013).

465 Christensen et al. (2000) based their study of Zackenberg Valley methane flux on chamber measurements from a c. 0.1 km^2 area of the northern part of Rylekærene (Fig. 2). The methane flux was measured with chambers on the five dominant vegetation types, and a mean flux for the valley was calculated by scaling fluxes to match the land cover classification of Bay (1998). The upscaled methane flux for the entire valley floor was 1.9 ± 0.7
470 $\text{mg m}^{-2} \text{ h}^{-1}$, which is higher than in any of the years in this study ($0.06 \pm 0.03 \text{ mg m}^{-2} \text{ h}^{-1}$ and $0.84 \pm 0.21 \text{ mg m}^{-2} \text{ h}^{-1}$). The distribution of land cover classes differs slightly between Bay (1998) and the HyMap dataset, which explains only some of the differences. However, a primary cause for the much higher valley estimate is the higher measured fluxes in the widespread Grassland class with a flux of $2.9 \pm 1.6 \text{ mg m}^{-2} \text{ h}^{-1}$ in Christensen et al. (2000), compared to $0.1 \pm 0.04 \text{ mg m}^{-2} \text{ h}^{-1}$ (SE converted from SD) in Tagesson et al. (2013). This difference impacts the valley flux, and if we substitute only the Grassland type flux from $0.1 \text{ mg m}^{-2} \text{ h}^{-1}$ to 2.9
475 $\text{mg m}^{-2} \text{ h}^{-1}$ in the upscaling to the entire valley floor, it would nearly double the methane flux in the valley. The substantial difference could indicate that grasslands in the marginal zones of fens have substantially elevated flux of methane in wet years and, hence, are key players in valley-wide interannual methane flux variability. Jørgensen et al. (2015) found a relatively high methane uptake on dry tundra, e.g., *Salix* snowbeds and Heath surfaces, compared to what has been found earlier. Including the uptake from Jørgensen et al. (2015) would
480 further limit the valley flux or even make the valley a net sink of methane in dry, warm years, as these surface classes combined account for more than 40 % of the valley floor (Table 2). As a result, the magnitude of the fluxes in Fig. 5 may be underestimated, as both positive and negative fluxes from Tagesson et al. (2013) are lower than found in both Christensen et al. (2000) and Jørgensen et al. (2015). Additionally, the year 2007 was chosen for the comparison because it exists in both datasets. However, the methane flux was exceptionally high
485 in that year (Fig. 3), which means that all other years in the time series were attributed to a lower flux. The valley methane fluxes are highly variable between years and do not show an increasing trend from the available data. Zackenberg Valley shows the potential for increased methane fluxes in the 21st century, as methane shows a positive correlation with temperatures which are expected to increase under the RCP8.5 climate scenario (Geng et al., 2019), similar to the trend of the rest of Greenland and the Arctic (AMAP, 2017).

490 Landscape-scale methane flux estimations are available from other subarctic and tundra sites (Table 3) in North America, Scandinavia, and Russia. The upscaled growing season fluxes range from 0.5 km^2 , extending from covering a few different ecosystems in a single site (Christensen et al., 2004) to large-scale estimates of fluxes covering up to $320,000 \text{ km}^2$ for the Hudson Bay Lowlands (Roulet et al., 1994). Mean methane fluxes in these



495 landscapes range from 0.3 to 3 mg m⁻² h⁻¹ across different scales and landscape types, covering growing seasons
of variable length with studies scattered across several decades. The mean methane flux for Zackenberg Valley
from 2006–2019 is 0.32 mg m⁻² h⁻¹ in the valley floor area (~16 km²) and 1.32 mg m⁻² h⁻¹ in the fen-rich
Rylekærene area (~1.3 km²). Hence, the results from Zackenberg Valley are in good agreement with
500 most studies in Table 3. All the included studies are either fully or partly based on chamber measurements and
upscaling with areal coverage of the surface classes, making them comparable to this study. Several of the
studies (Bartlett et al., 1992; Roulet et al., 1994; Bosse and Frenzel, 2001; Hartley et al., 2015) estimated the
landscape methane fluxes based on observations from a single year. The remaining studies combine
observations from multiple years or studies to a flux estimate from each surface cover class (Christensen et al.,
505 2004; Schneider et al., 2009; Andresen et al., 2017; Morozumi et al., 2019). Flux measurements from several
years lead to more robust landscape flux estimates, as the fluxes are highly variable between years, as the present
study also shows.

The large differences in study area size and composition are ultimately determining the mean methane flux
estimates of the landscape, which makes direct comparisons between sites difficult. For instance, the mean
510 landscape flux found in this study is nearly four times greater for the fen rich Rylekærene study area, which is
entirely contained in the valley floor study area. On an even larger scale, the entire northeast Greenland acts as
a net sink of methane, as Jørgensen et al. (2015) found a mean methane flux of ~-0.08 mg m⁻² h⁻¹ in their
10,675 km² study area.

515 **Table 3: Comparison of landscape-integrated growing season methane flux for various subarctic and Arctic sites with a
minimum size of 0.5 km².**

Publication	Location	Climate zone	Landscape type	Mean flux (mg CH ₄ m ⁻² h ⁻¹)	Area size (km ²)
Bartlett et al. (1992)	Yukon-Kuskokwim Delta (Alaska, USA)	Subarctic	Wetlands	1.8	97,400
Roulet et al. (1994)	Hudson Bay Lowlands (Ontario-Manitoba, Canada)	Subarctic	Wetlands	0.8	320,000
Bosse and Frenzel (2001)	Yenisey River (W Siberia, Russia)	Subarctic	Mire, wetlands, and Pine forest	1	361
Christensen et al. (2004)	Stordalen (Norrbotten, Sweden)	Subarctic	Mire	2.7 to 3.0	0.5
Heikkinen et al. (2004)	Lek Vorkuta (N Komi, Russia)	Arctic tundra	Heath, peatland, and Salix	0.6	114
Schneider et al. (2009)	Lena Delta (N Siberia, Russia)	Arctic tundra	Wetlands	0.4	29,036
Hartley et al. (2015)	Kevo (Lapland, Finland)	Subarctic	Aapa mires and birch forest	0.3 to 0.4	100
Andresen et al. (2017)	Utqiagvik Peninsula (Alaska, USA)	Arctic tundra	Arctic coastal plains	0.6	1779
Morozumi et al. (2019)	Indigirka (NE Siberia, Russia)	Arctic tundra	Larch forest, shrubs, and wetlands	1.6	96

Several other studies have applied the EC method for ecosystem methane flux measurements at landscape-scale
in the Arctic, e.g., Fan et al. (1992); Sachs et al. (2008); Wille et al. (2008); Jackowicz-Korczynski et al. (2010);
520 Parmentier et al. (2011); Taylor et al. (2018). While the EC method integrates ecosystem fluxes at high temporal
resolution by nonintrusive means and is preferred for these reasons, those studies are generally restricted to
smaller areas less than 0.5 km². Ecosystem fluxes from these studies range between ~0.1 to 6.2 mg m⁻² h⁻¹, with
the lowest growing season fluxes measured at an upland tussock tundra site by Eight Mile Lake in Alaska



(Taylor et al., 2018) and the highest fluxes measured in a mire in Stordalen, north Sweden (Jackowicz-
525 Korczynski et al., 2010). Mean growing season fluxes found in Zackenberg using the EC method are within this
interval (Friborg et al., 2000; Tagesson et al., 2012).

4.3 Landscape methane flux in a changing climate

A warming trend in both air and soil temperatures has been observed for Zackenberg Valley (Abermann et al.,
2017; Christensen et al., 2020b). The increase in temperatures has contributed to the destabilization of
530 permafrost, leading to several active periglacial landforms in recent years (Docherty et al., 2017; Cable et al.,
2018; Christensen et al., 2020b). Modeling results show higher soil temperatures and a deepening of the AL in
Zackenberg in the future (Christiansen et al., 2008; Westermann et al., 2015). Increasing temperatures are
expected to impact both methane flux and surface erosion in the Arctic (Geng et al., 2019; Schuur et al., 2015),
which is also likely for Zackenberg Valley. The emergence of several active erosion sites along the Zackenberg
535 River in recent years could be an initial step towards increased erosion activity in the 21st century in the valley.
In 2019, after the disappearance of methane-rich ice-wedges in the previous year, carbon-rich soils had been
washed out from the gully, leaving a silt-organic mix with limited potential for methane emission in the area
(Christensen et al., 2020b). This study defines two erosion scenarios to illustrate the sensitivity of methane flux
to land cover changes on a valley-scale. We hypothesize large-scale linear growth in eroded areas along the
540 banks of the Zackenberg River by the late 21st century (i.e., 2081–2100), characterized by the changes in fluxes
like those observed in the gully area in 2019. Increased erosion would transform large areas with limited
methane emission and uptake into well-drained, low emission eroded surfaces. These two erosion scenarios are
unlikely, but they are valuable as a sensitivity study illustrating the difference in importance of increasing
temperatures relative to eroding surfaces. In this example, a backward gully erosion area was studied, but
545 erosion caused by the Zackenberg River, and especially GLOFs, appear to have a larger impact on the erosion
of the riverbanks (Tomczyk et al., 2020) and would most likely have a similar effect on methane fluxes. Further,
erosion of the riverbanks is more pronounced on the outer banks of the river bends (Tomczyk et al., 2020).
Backward gully erosion may be limited to ice-rich parts of the riverbanks, but the extent of these is largely
unknown along the Zackenberg River inside the study area (Cable et al., 2018).

550

Even large-scale erosion along the river would have a limited impact on the mean valley methane flux, reducing
the flux by less than 1 % on average between 2041–2060, while surface erosion gradually progresses toward
the first third of 25 m or 100 m, respectively. The reduction becomes more pronounced between 2081–2100, as
eroded areas would develop further inland and cause disturbances to areas dominated by fen. When fen areas
555 are eroded, the flux is expected to decline, causing the area to become a relative sink of methane. The erosion
could cause the mean methane fluxes of the valley to decrease by -0.7% and -7.8% in the late period, with 25
m and 100 m eroded areas along the river.



The resulting changes in flux following erosion are minor relative to the considerable uncertainty in the general shift in methane for the valley following an increase in temperature. In this case, methane fluxes were measured
560 in a gully, which becomes more drained with a loss of organic soils from the surface after an erosion event (Christensen et al., 2020b). Fluvial erosion of vegetated riverbanks would most likely have a similar impact on methane fluxes when organic soils and vegetation are eroded.

The gully described in this study has likely formed as a direct consequence of pronounced lateral erosion from the river, which steepened the gully, allowing for increased drainage of water and sediments. The increased
565 drainage exposed more and more of the ice-wedges and frozen soils, which later thawed and flowed out through the steeper gully. The gully shares characteristics with thermokarst gullies, a common type of thermokarst erosion, including extent, depth, and shape (Jorgenson et al., 2008). Abrupt thaw, including both gullies and thermokarst areas, can take different forms and affect the surface methane flux through disturbances in both vegetation and hydrology (Turetsky et al., 2020). Olefeldt et al. (2016) use a definition of thermokarst
570 landscapes, including thermo-erosion gullies characterized by lateral movement of sediments, similar to the gully described in our study. Olefeldt et al. (2016) estimate that ~20 % of land areas in the northern permafrost zone are thermokarst landscapes, meaning they are either currently characterized by soil settlement or erosion or prone to developing into thermokarst landforms in the future. Thermokarst landforms have diverse impacts on a landscape, dependent on their type (Kokelj and Jorgenson, 2013). They could form abruptly and rapidly
575 responding to increasing temperatures (Farquharson et al., 2019; Lewkowicz and Way, 2019). Wickland et al. (2020) found a 42 % increase in growing season methane flux from 1949–2018 in a wet polygonal tundra after an increase in thermokarst erosion of ice-wedges. Thermokarst lakes cover large areas across the Boreal zone and in the Arctic and have been reported to be substantial emitters of methane (Wik et al., 2016; Walter Anthony et al., 2018; Engram et al., 2020). These findings contrast the results from this study, where erosion causes
580 draining and loss of organic material. Wik et al. (2016) found a mean flux, combining diffusion and ebullition, of ~3.7 mg m⁻² h⁻¹ from thermokarst lakes in the ice-free season. Walter Anthony et al. (2018) found an accelerating increase in methane fluxes from thermokarst lakes in their modeling of methane in the 21st for the circumpolar region, which also contrasts the impacts from the gully found in Zackenberg Valley. It should be noted that there is a difference in the ‘receiving end’ of the gully formation between our study and these
585 thermokarst lake studies as the drainage in the Zackenberg valley goes straight out in the major river with no stagnant reservoir between.

In our calculation of landscape methane fluxes to changes in surface cover, eroded areas stay unvegetated for the remainder of the century. Still, eroded areas may partly be revegetated after stabilizing, which could change the size of the relative sink shown in Fig. 6. Further, methane oxidation could increase the sink in upland areas
590 during the 21st century (Jørgensen et al., 2015; Oh et al., 2020), which could offset some of the increase in mean flux in Zackenberg Valley.



5 Conclusions

In this study, we have summarized 14 measurement-years of methane fluxes and several short-term campaigns, which provide a unique insight into the large variability in methane fluxes in a high Arctic tundra landscape of Zackenber
595 Zackenber Valley. We have combined July–August measurements from a monitoring site running from 2006–2019 with detailed single-year measurements of the most common vegetation types in the valley to estimate valley-wide methane fluxes over the period. For the valley, the net emission of methane in July–August shows differences by a factor of 10 between individual years (2006–2019). Consistently dry or wet surfaces may remain relatively stable in terms of methane fluxes over the period, as indicated by the data from previous site-
600 specific campaigns in the valley. However, the large areas covering the boundary between these host highly variable methane fluxes significantly impacting methane fluxes at the landscape-scale. Future multiyear campaigns should focus on measuring the full gradient from wet fens to dry heath to improve estimations of landscape methane fluxes, as the fluxes from different surface classes may respond differently to changes in environmental conditions, such as moisture, temperature, snow cover.

605 Observations from recently eroded gully revealed a small source of methane in this type of landscape. Rapid export of carbon-rich soils and an effective drainage system in the gully are likely the main reasons for the limited methane fluxes.

With rising temperatures in Zackenber Valley, methane emissions are expected to increase drastically during the 21st century. The warming increases permafrost thaw, which could increase surface erosion in the valley.
610 When compared, our findings show the increase in methane emission from undisturbed fen areas has a much larger impact on the valley-wide fluxes than surface erosion, even if riverbanks are heavily eroded. Increased erosion could offset some of the rise in methane fluxes from the valley, but this would require large-scale impacts on vegetated surfaces.

This study shows the importance of multiyear methane monitoring with wide spatial coverage, as interannual
615 variability is substantial when considering a full composite landscape even in a single valley in the Arctic.

Data and code availability

Data from the GEM ClimateBasis and GeoBasis Zackenber subprograms used in this manuscript are free and open data, available at <https://data.g-e-m.dk/> (registration needed). The data are licensed with terms of use under the Creative Commons CC-BY-SA license. Processed data and scripts used for the analyses are available at
620 https://github.com/schellers/Multidecadal-growing-season-fluxes-of-a-high-Arctic-tundra/raw/main/Data_and_code_Multidecadal_growing_season_fluxes_of_a_high_Arctic_tundra.zip.

Direct links to the GEM data sources are listed here:

AC Water level automatic: <https://doi.org/10.17897/mj7b-z461>

AC Water level manual: <https://doi.org/10.17897/6hcp-m521>



625 Air temperature, 200cm – 60min average: <https://doi.org/10.17897/xv96-hc57>

Flux monitoring – AC: <https://doi.org/10.17897/430p-ds31>

Mix-1 Soil moisture: <https://doi.org/10.17897/ennb-t831>

Snow cover (Central area): <https://doi.org/10.17897/499c-h459>

Soil temperature, 20cm – 60min average: <https://doi.org/10.17897/xw7c-na36>

630 Author contribution

JHS, MM, and TRC designed the study, and JHS performed the analyses and created figures and tables. HHC helped to interpret the geomorphological processes. JHS wrote the manuscript with contributions from all co-authors.

Competing interests

635 The authors declare that they have no conflict of interest.

Acknowledgments

This study was supported by the Faculty of Science and Technology and the thematic centers iCLIMATE and ARC at Aarhus University. The authors furthermore acknowledge the use of data from the Greenland Ecosystem Monitoring (GEM) database and are grateful for field support provided by the Zackenberg

640 Research Station.

References

Abermann, J., Hansen, B., Lund, M., Wacker, S., Karami, M., and Cappelen, J.: Hotspots and key periods of Greenland climate change during the past six decades, *Ambio*, 46, 3-11, doi: 10.1007/s13280-016-0861-y, 2017.

645 AMAP: Snow, Water and Permafrost in the Arctic (SWIPA) 2017, Oslo, Norway, 269 pp., 2017.

Andresen, C. G., Lara, M. J., Tweedie, C. E., and Loughheed, V. L.: Rising plant-mediated methane emissions from arctic wetlands, *Global Change Biology*, 23, 1128-1139, doi: 10.1111/gcb.13469, 2017.

650 Bartlett, K. B., Crill, P. M., Sass, R. L., Harriss, R. C., and Dise, N. B.: Methane emissions from tundra environments in the Yukon-Kuskokwim delta, Alaska, *Journal of Geophysical Research*, 97, 16645-16660, doi: 10.1029/91jd00610, 1992.

655 Bay, C.: Vegetation mapping of Zackenberg valley, northeast Greenland, Danish Polar Center and Botanical Museum, University of Copenhagen, 1998.



- Bosse, U., and Frenzel, P.: CH₄ emissions from a West Siberian mire, *Suo*, 52, 99-114, 2001.
- 660 Cable, S., Christiansen, H. H., Westergaard-Nielsen, A., Kroon, A., and Elberling, B.: Geomorphological and cryostratigraphical analyses of the Zackenberg Valley, NE Greenland and significance of Holocene alluvial fans, *Geomorphology*, 303, 504-523, doi: 10.1016/j.geomorph.2017.11.003, 2018.
- Christensen, T. R.: Methane emission from Arctic tundra, *Biogeochemistry*, 21, 117-139, doi: 10.1007/bf00000874, 1993.
- 665 Christensen, T. R., Friborg, T., Sommerkorn, M., Kaplan, J., Illeris, L., Søgaard, H., Nordstrøm, C., and Jonasson, S.: Trace gas exchange in a high-arctic valley 1. Variations in CO₂ and CH₄ flux between tundra vegetation types, *Global Biogeochemical Cycles*, 14, 701-713, doi: 10.1029/1999gb001134, 2000.
- 670 Christensen, T. R., Johansson, T. R., Akerman, H. J., Mastepanov, M., Malmer, N., Friborg, T., Crill, P., and Svensson, B. H.: Thawing sub-arctic permafrost: Effects on vegetation and methane emissions, *Geophysical Research Letters*, 31, doi: 10.1029/2003gl018680, 2004.
- Christensen, T. R.: Climate science: Understand Arctic methane variability, *Nature*, 509, 279-281, doi: 10.1038/509279a, 2014.
- 675 Christensen, T. R., Arndal, M. F., and Topp-Jørgensen, E.: Greenland Ecosystem Monitoring Annual Report Cards 2019, DCE – Danish Centre for Environment and Energy, Aarhus University, Aarhus, Denmark, 40 pp, 2020a.
- 680 Christensen, T. R., Lund, M., Skov, K., Abermann, J., López-Blanco, E., Scheller, J., Scheel, M., Jackowicz-Korczynski, M., Langley, K., Murphy, M. J., and Mastepanov, M.: Multiple Ecosystem Effects of Extreme Weather Events in the Arctic, *Ecosystems*, doi: 10.1007/s10021-020-00507-6, 2020b.
- 685 Christiansen, H. H., Sigsgaard, C., Humlum, O., Rasch, M., and Hansen, B. U.: Permafrost and Periglacial Geomorphology at Zackenberg, in: *High-Arctic Ecosystem Dynamics in a Changing Climate*, *Advances in Ecological Research*, 151-174, 2008.
- 690 COWI: eBee saves the day: mapping Greenland's Zackenberg Research Station https://www.sensefly.com/app/uploads/2017/11/eBee_saves_day_mapping_greenlands_zackenberg_research_station.pdf, 2015.
- 695 Crill, P. M., Bartlett, K. B., Harriss, R. C., Gorham, E., Verry, E. S., Sebacher, D. I., Madzar, L., and Sanner, W.: Methane flux from Minnesota peatlands, *Global Biogeochemical Cycles*, 2, 371-384, doi: 10.1029/gb002i004p00371, 1988.
- Docherty, C. L., Hannah, D. M., Riis, T., Leth, S. R., and Milner, A. M.: Large thermo-erosional tunnel for a river in northeast Greenland, *Polar Science*, 14, 83-87, doi: 10.1016/j.polar.2017.08.001, 2017.
- 700 Ehhalt, D. H.: The atmospheric cycle of methane, *Tellus*, 26, 58-70, doi: 10.3402/tellusa.v26i1-2.9737, 1974.



- 705 Elberling, B., Tamstorf, M. P., Michelsen, A., Arndal, M. F., Sigsgaard, C., Illeris, L., Bay, C., Hansen, B. U., Christensen, T. R., Hansen, E. S., Jakobsen, B. H., and Beyens, L.: Soil and Plant Community-Characteristics and Dynamics at Zackenberg, in: *Advances in Ecological Research: High-Arctic Ecosystem Dynamics in a Changing Climate*, Elsevier, 223-248, 2008.
- Engram, M., Anthony, K. M. W., Sachs, T., Kohnert, K., Serafimovich, A., Grosse, G., and Meyer, F. J.: Remote sensing northern lake methane ebullition, *Nature Climate Change*, doi: 10.1038/s41558-020-0762-8, 2020.
- 710 Falk, J. M., Schmidt, N. M., and Ström, L.: Effects of simulated increased grazing on carbon allocation patterns in a high arctic mire, *Biogeochemistry*, 119, 229-244, doi: 10.1007/s10533-014-9962-5, 2014.
- Falk, J. M., Schmidt, N. M., Christensen, T. R., and Ström, L.: Large herbivore grazing affects the vegetation structure and greenhouse gas balance in a high arctic mire, *Environ Res Lett*, 10, doi: 10.1088/1748-9326/10/4/045001, 2015.
- 715 Falk, J. M., Schmidt, N. M., Christensen, T. R., and Ström, L.: Large herbivore grazing affects the vegetation structure and greenhouse gas balance in a high arctic mire, *Environ Res Lett*, 10, doi: 10.1088/1748-9326/10/4/045001, 2015.
- Fan, S. M., Wofsy, S. C., Bakwin, P. S., Jacob, D. J., Anderson, S. M., Keibarian, P. L., McManus, J. B., Kolb, C. E., and Fitzjarrald, D. R.: Micrometeorological measurements of CH₄ and CO₂ exchange between the atmosphere and subarctic tundra, *Journal of Geophysical Research*, 97, 16627-16643, doi: 10.1029/91jd02531, 1992.
- 720 Fan, S. M., Wofsy, S. C., Bakwin, P. S., Jacob, D. J., Anderson, S. M., Keibarian, P. L., McManus, J. B., Kolb, C. E., and Fitzjarrald, D. R.: Micrometeorological measurements of CH₄ and CO₂ exchange between the atmosphere and subarctic tundra, *Journal of Geophysical Research*, 97, 16627-16643, doi: 10.1029/91jd02531, 1992.
- Farquharson, L. M., Romanovsky, V. E., Cable, W. L., Walker, D. A., Kokelj, S. V., and Nicolsky, D.: Climate Change Drives Widespread and Rapid Thermokarst Development in Very Cold Permafrost in the Canadian High Arctic, *Geophysical Research Letters*, 46, 6681-6689, doi: 10.1029/2019gl082187, 2019.
- 725 Farquharson, L. M., Romanovsky, V. E., Cable, W. L., Walker, D. A., Kokelj, S. V., and Nicolsky, D.: Climate Change Drives Widespread and Rapid Thermokarst Development in Very Cold Permafrost in the Canadian High Arctic, *Geophysical Research Letters*, 46, 6681-6689, doi: 10.1029/2019gl082187, 2019.
- Friborg, T., Christensen, T. R., Hansen, B. U., Nordstrøm, C., and Søgaard, H.: Trace gas exchange in a high-Arctic valley 2. Landscape CH₄ fluxes measured and modeled using eddy correlation data, *Global Biogeochemical Cycles*, 14, 715-723, doi: 10.1029/1999gb001136, 2000.
- 730 Geng, M. S., Christensen, J. H., and Christensen, T. R.: Potential future methane emission hot spots in Greenland, *Environ Res Lett*, 14, 035001, doi: 10.1088/1748-9326/aaf34b, 2019.
- Grøndahl, L., Friborg, T., Christensen, T. R., Ekberg, A., Elberling, B., Illeris, L., Nordstrøm, C., Rennermalm, Å., Sigsgaard, C., and Søgaard, H.: Spatial and inter-annual variability of trace gas fluxes in a heterogeneous high-arctic landscape, in: *Advances in Ecological Research: High-Arctic Ecosystem Dynamics in a Changing Climate*, Elsevier, 473-498, 2008.
- 735 Grøndahl, L., Friborg, T., Christensen, T. R., Ekberg, A., Elberling, B., Illeris, L., Nordstrøm, C., Rennermalm, Å., Sigsgaard, C., and Søgaard, H.: Spatial and inter-annual variability of trace gas fluxes in a heterogeneous high-arctic landscape, in: *Advances in Ecological Research: High-Arctic Ecosystem Dynamics in a Changing Climate*, Elsevier, 473-498, 2008.
- Hansen, B. U., Sigsgaard, C., Rasmussen, L., Cappelen, J., Hinkler, J., Mernild, S. H., Petersen, D., Tamstorf, M. P., Rasch, M., and Hasholt, B.: Present-Day Climate at Zackenberg, in: *Advances in Ecological Research: High-Arctic Ecosystem Dynamics in a Changing Climate*, Elsevier, 111-149, 2008.
- 740 Hansen, B. U., Sigsgaard, C., Rasmussen, L., Cappelen, J., Hinkler, J., Mernild, S. H., Petersen, D., Tamstorf, M. P., Rasch, M., and Hasholt, B.: Present-Day Climate at Zackenberg, in: *Advances in Ecological Research: High-Arctic Ecosystem Dynamics in a Changing Climate*, Elsevier, 111-149, 2008.
- Hartley, I. P., Hill, T. C., Wade, T. J., Clement, R. J., Moncrieff, J. B., Prieto-Blanco, A., Disney, M. I., Huntley, B., Williams, M., Howden, N. J. K., Wookey, P. A., and Baxter, R.: Quantifying landscape-level methane fluxes in subarctic Finland using a multiscale approach, *Global Change Biology*, 21, 3712-3725, doi: 10.1111/gcb.12975, 2015.
- 745 Hartley, I. P., Hill, T. C., Wade, T. J., Clement, R. J., Moncrieff, J. B., Prieto-Blanco, A., Disney, M. I., Huntley, B., Williams, M., Howden, N. J. K., Wookey, P. A., and Baxter, R.: Quantifying landscape-level methane fluxes in subarctic Finland using a multiscale approach, *Global Change Biology*, 21, 3712-3725, doi: 10.1111/gcb.12975, 2015.
- Heikkinen, J. E. P., Virtanen, T., Huttunen, J. T., Elsakov, V., and Martikainen, P. J.: Carbon balance in East European tundra, *Global Biogeochemical Cycles*, 18, doi: 10.1029/2003gb002054, 2004.



- 750 IPCC: Climate Change The IPCC Scientific Assessment, Intergovernmental Panel on Climate Change, Cambridge, 1990.
- Jackowicz-Korczynski, M., Christensen, T. R., Bäckstrand, K., Crill, P., Friborg, T., Mastepanov, M., and Ström, L.: Annual cycle of methane emission from a subarctic peatland, *Journal of Geophysical Research*, 115, G02009, doi: 10.1029/2008jg000913, 2010.
- 755 Joabsson, A., and Christensen, T. R.: Methane emissions from wetlands and their relationship with vascular plants: an Arctic example, *Global Change Biology*, 7, 919-932, doi: 10.1046/j.1354-1013.2001.00044.x, 2001.
- 760 Jorgenson, M. T., Schur, Y. L., and Osterkamp, T. E.: Thermokarst in Alaska, Ninth International Conference on Permafrost, Fairbanks, 2008, 869-876,
- Jørgensen, C. J., Lund Johansen, K. M., Westergaard-Nielsen, A., and Elberling, B.: Net regional methane sink in High Arctic soils of northeast Greenland, *Nature Geoscience*, 8, 20-23, doi: 10.1038/ngeo2305, 2015.
- 765 Kokelj, S. V., and Jorgenson, M. T.: Advances in Thermokarst Research, *Permafrost and Periglacial Processes*, 24, 108-119, doi: 10.1002/ppp.1779, 2013.
- 770 Lewkowicz, A. G., and Way, R. G.: Extremes of summer climate trigger thousands of thermokarst landslides in a High Arctic environment, *Nature Communications*, 10, 1329, doi: 10.1038/s41467-019-09314-7, 2019.
- Livingston, G., and Hutchinson, G.: Enclosure-based measurement of trace gas exchange: applications and sources of error, in: *Biogenic trace gases: measuring emissions from soil and water*, edited by: Matson, P. A. a. H., R.C., Blackwell Science Ltd., 14-51, 1995.
- 775 Mastepanov, M., Sigsgaard, C., Dlugokencky, E. J., Houweling, S., Ström, L., Tamstorf, M. P., and Christensen, T. R.: Large tundra methane burst during onset of freezing, *Nature*, 456, 628-630, doi: 10.1038/nature07464, 2008.
- 780 Mastepanov, M., Sigsgaard, C., Mastepanov, M., Ström, L., Tamstorf, M. P., Lund, M., and Christensen, T. R.: Revisiting factors controlling methane emissions from high-Arctic tundra, *Biogeosciences*, 10, 5139-5158, doi: 10.5194/bg-10-5139-2013, 2013.
- 785 Mastepanov, M., Pirk, N., Lopez-Blanco, E., Skov, K., Rudd, D., Jackowicz-Korczynski, M., Tamstorf, M., Scheller, J., and Christensen, T. R.: Fifteen years of methane flux measurements in high-arctic tundra, in prep.
- Meltofte, H., Christensen, T. R., Elberling, B., Forchhammer, M. C., and Rasch, M.: Introduction, in: *Advances in Ecological Research: High-Arctic Ecosystem Dynamics in a Changing Climate*, Elsevier, 1-12, 2008.
- 790 Meltofte, H., and Rasch, M.: The Study Area at Zackenberg, in: *Advances in Ecological Research: High-Arctic Ecosystem Dynamics in a Changing Climate*, Elsevier, 101-110, 2008.



- 795 Morozumi, T., Shingubara, R., Suzuki, R., Kobayashi, H., Tei, S., Takano, S., Fan, R., Liang, M., Maximov, T., and Sugimoto, A.: Estimating methane emissions using vegetation mapping in the taiga–tundra boundary of a north-eastern Siberian lowland, *Tellus B: Chemical and Physical Meteorology*, 71, 1581004, doi: 10.1080/16000889.2019.1581004, 2019.
- 800 Morrissey, L. A., and Livingston, G. P.: Methane emissions from Alaska Arctic tundra: An assessment of local spatial variability, *Journal of Geophysical Research: Atmospheres*, 97, 16661-16670, doi: 10.1029/92jd00063, 1992.
- 805 Oh, Y., Zhuang, Q. L., Liu, L. C., Welp, L. R., Lau, M. C. Y., Onstott, T. C., Medvigy, D., Bruhwiler, L., Dlugokencky, E. J., Hugelius, G., D'Imperio, L., and Elberling, B.: Reduced net methane emissions due to microbial methane oxidation in a warmer Arctic, *Nature Climate Change*, 10, 317-321, doi: 10.1038/s41558-020-0734-z, 2020.
- 810 Olefeldt, D., Turetsky, M. R., Crill, P. M., and McGuire, A. D.: Environmental and physical controls on northern terrestrial methane emissions across permafrost zones, *Global Change Biology*, 19, 589-603, doi: 10.1111/gcb.12071, 2013.
- 815 Olefeldt, D., Goswami, S., Grosse, G., Hayes, D., Hugelius, G., Kuhry, P., McGuire, A. D., Romanovsky, V. E., Sannel, A. B., Schuur, E. A., and Turetsky, M. R.: Circumpolar distribution and carbon storage of thermokarst landscapes, *Nature Communications*, 7, 13043, doi: 10.1038/ncomms13043, 2016.
- 825 Palmtag, J., Hugelius, G., Lashchinskiy, N., Tamstorf, M. P., Richter, A., Elberling, B., and Kuhry, P.: Storage, landscape distribution, and burial history of soil organic matter in contrasting areas of continuous permafrost, Arctic, Antarctic, and Alpine Research, 47, 71-88, doi: 10.1657/aaar0014-027, 2015.
- 820 Parmentier, F., Van Huissteden, J., Van Der Molen, M., Schaepman-Strub, G., Karsanaev, S., Maximov, T., and Dolman, A.: Spatial and temporal dynamics in eddy covariance observations of methane fluxes at a tundra site in northeastern Siberia, *Journal of Geophysical Research*, 116, doi: 10.1029/2010jg001637, 2011.
- 825 Pedersen, S. H., Tamstorf, M. P., Abermann, J., Westergaard-Nielsen, A., Lund, M., Skov, K., Sigsgaard, C., Mylius, M. R., Hansen, B. U., Liston, G. E., and Schmidt, N. M.: Spatiotemporal Characteristics of Seasonal Snow Cover in Northeast Greenland from in Situ Observations, *Arctic, Antarctic, and Alpine Research*, 48, 653-671, doi: 10.1657/aaar0016-028, 2016.
- 830 Pirk, N., Mastepanov, M., Parmentier, F. J. W., Lund, M., Crill, P., and Christensen, T. R.: Calculations of automatic chamber flux measurements of methane and carbon dioxide using short time series of concentrations, *Biogeosciences*, 13, 903-912, doi: 10.5194/bg-13-903-2016, 2016a.
- 835 Pirk, N., Tamstorf, M. P., Lund, M., Mastepanov, M., Pedersen, S. H., Mylius, M. R., Parmentier, F. J. W., Christiansen, H. H., and Christensen, T. R.: Snowpack fluxes of methane and carbon dioxide from high Arctic tundra, *Journal of Geophysical Research: Biogeosciences*, 121, 2886-2900, doi: 10.1002/2016jg003486, 2016b.
- 840 Roulet, N. T., Jano, A., Kelly, C., Klinger, L., Moore, T., Protz, R., Ritter, J., and Rouse, W.: Role of the Hudson Bay lowland as a source of atmospheric methane, *Journal of Geophysical Research: Atmospheres*, 99, 1439-1454, doi: 10.1029/93jd00261, 1994.



- Sachs, T., Wille, C., Boike, J., and Kutzbach, L.: Environmental controls on ecosystem-scale CH₄ emission from polygonal tundra in the Lena River Delta, Siberia, *Journal of Geophysical Research*, 113, doi: 10.1029/2007jg000505, 2008.
- 845 Schneider, J., Grosse, G., and Wagner, D.: Land cover classification of tundra environments in the Arctic Lena Delta based on Landsat 7 ETM+ data and its application for upscaling of methane emissions, *Remote Sensing of Environment*, 113, 380-391, doi: 10.1016/j.rse.2008.10.013, 2009.
- Schuur, E. A., McGuire, A. D., Schadel, C., Grosse, G., Harden, J. W., Hayes, D. J., Hugelius, G., Koven, C. D., Kuhry, P., Lawrence, D. M., Natali, S. M., Olefeldt, D., Romanovsky, V. E., Schaefer, K., Turetsky, M. R., Treat, C. C., and Vonk, J. E.: Climate change and the permafrost carbon feedback, *Nature*, 520, 171-179, doi: 10.1038/nature14338, 2015.
- 850 Shakhova, N., Semiletov, I., Leifer, I., Sergienko, V., Salyuk, A., Kosmach, D., Chernykh, D., Stubbs, C., Nicolsky, D., Tumskey, V., and Gustafsson, Ö.: Ebullition and storm-induced methane release from the East Siberian Arctic Shelf, *Nature Geoscience*, 7, 64-70, doi: 10.1038/ngeo2007, 2014.
- 855 Stiegler, C., Lund, M., Christensen, T. R., Mastepanov, M., and Lindroth, A.: Two years with extreme and little snowfall: effects on energy partitioning and surface energy exchange in a high-Arctic tundra ecosystem, *The Cryosphere*, 10, 1395-1413, doi: 10.5194/tc-10-1395-2016, 2016.
- 860 Ström, L., Ekberg, A., Mastepanov, M., and Christensen, T. R.: The effect of vascular plants on carbon turnover and methane emissions from a tundra wetland, *Global Change Biology*, 9, 1185-1192, doi: 10.1046/j.1365-2486.2003.00655.x, 2003.
- 865 Ström, L., Tagesson, T., Mastepanov, M., and Christensen, T. R.: Presence of *Eriophorum scheuchzeri* enhances substrate availability and methane emission in an Arctic wetland, *Soil Biol Biochem*, 45, 61-70, doi: 10.1016/j.soilbio.2011.09.005, 2012.
- 870 Ström, L., Falk, J. M., Skov, K., Jackowicz-Korczynski, M., Mastepanov, M., Christensen, T. R., Lund, M., and Schmidt, N. M.: Controls of spatial and temporal variability in CH₄ flux in a high arctic fen over three years, *Biogeochemistry*, 125, 21-35, doi: 10.1007/s10533-015-0109-0, 2015.
- 875 Svensson, B. H., and Rosswall, T.: In situ Methane Production from Acid Peat in Plant Communities with Different Moisture Regimes in a Subarctic Mire, *Oikos*, 43, 341-350, doi: 10.2307/3544151, 1984.
- Søgaard, H., Nordstrøm, C., Friborg, T., and Hansen, B. U.: Trace gas exchange in a high-arctic valley 3. Integrating and scaling CO₂ fluxes from canopy to landscape using flux data, footprint modeling, and remote sensing, *Global Biogeochemical Cycles*, 14, 725-744, doi: 10.1029/1999gb001137, 2000.
- 880 Søndergaard, J., Tamstorf, M., Elberling, B., Larsen, M. M., Mylius, M. R., Lund, M., Abermann, J., and Rigét, F.: Mercury exports from a High-Arctic river basin in Northeast Greenland (74°N) largely controlled by glacial lake outburst floods, *Science of The Total Environment*, 514, 83-91, doi: 10.1016/j.scitotenv.2015.01.097, 2015.
- 885 Tagesson, T., Mølder, M., Mastepanov, M., Sigsgaard, C., Tamstorf, M. P., Lund, M., Falk, J. M., Lindroth, A., Christensen, T. R., and Ström, L.: Land-atmosphere exchange of methane from soil thawing to soil freezing in



- a high-Arctic wet tundra ecosystem, *Global Change Biology*, 18, 1928-1940, doi: 10.1111/j.1365-2486.2012.02647.x, 2012.
- 890 Tagesson, T., Mastepanov, M., Mölder, M., Tamstorf, M. P., Eklundh, L., Smith, B., Sigsgaard, C., Lund, M., Ekberg, A., Falk, J. M., Friberg, T., Christensen, T. R., and Ström, L.: Modelling of growing season methane fluxes in a high-Arctic wet tundra ecosystem 1997-2010 using in situ and high-resolution satellite data, *Tellus B: Chemical and Physical Meteorology*, 65, doi: 10.3402/tellusb.v65i0.19722, 2013.
- 895 Taylor, M. A., Celis, G., Ledman, J. D., Bracho, R., and Schuur, E. A. G.: Methane Efflux Measured by Eddy Covariance in Alaskan Upland Tundra Undergoing Permafrost Degradation, *Journal of Geophysical Research: Biogeosciences*, 123, 2695-2710, doi: 10.1029/2018jg004444, 2018.
- 900 Thornton, B. F., Prytherch, J., Andersson, K., Brooks, I. M., Salisbury, D., Tjernström, M., and Crill, P. M.: Shipborne eddy covariance observations of methane fluxes constrain Arctic sea emissions, *Science advances*, 6, eaay7934, doi: 10.1126/sciadv.aay7934, 2020.
- 905 Tomczyk, A. M., and Ewertowski, M. W.: UAV-based remote sensing of immediate changes in geomorphology following a glacial lake outburst flood at the Zackenberg river, northeast Greenland, *Journal of Maps*, 16, 86-100, doi: 10.1080/17445647.2020.1749146, 2020.
- 910 Tomczyk, A. M., Ewertowski, M. W., and Carrivick, J. L.: Geomorphological impacts of a glacier lake outburst flood in the high arctic Zackenberg River, NE Greenland, *Journal of Hydrology*, 591, 125300, doi: 10.1016/j.jhydrol.2020.125300, 2020.
- 915 Turetsky, M. R., Abbott, B. W., Jones, M. C., Anthony, K. W., Olefeldt, D., Schuur, E. A. G., Grosse, G., Kuhry, P., Hugelius, G., Koven, C., Lawrence, D. M., Gibson, C., Sannel, A. B. K., and McGuire, A. D.: Carbon release through abrupt permafrost thaw, *Nature Geoscience*, 13, 138-145, doi: 10.1038/s41561-019-0526-0, 2020.
- 920 Walter Anthony, K., Schneider von Deimling, T., Nitze, I., Frohling, S., Emond, A., Daanen, R., Anthony, P., Lindgren, P., Jones, B., and Grosse, G.: 21st-century modeled permafrost carbon emissions accelerated by abrupt thaw beneath lakes, *Nature Communications*, 9, 3262, doi: 10.1038/s41467-018-05738-9, 2018.
- 925 Westermann, S., Elberling, B., Højlund Pedersen, S., Stendel, M., Hansen, B. U., and Liston, G. E.: Future permafrost conditions along environmental gradients in Zackenberg, Greenland, *The Cryosphere*, 9, 719-735, doi: 10.5194/tc-9-719-2015, 2015.
- 925 Whalen, S. C., and Reeburgh, W. S.: A methane flux time series for tundra environments, *Global Biogeochemical Cycles*, 2, 399-409, doi: 10.1029/gb002i004p00399, 1988.
- 930 Wickland, K. P., Jorgenson, M. T., Koch, J. C., Kanevskiy, M., and Striegl, R. G.: Carbon dioxide and methane flux in a dynamic Arctic tundra landscape: Decadal-scale impacts of ice-wedge degradation and stabilization, *Geophysical Research Letters*, 47, e2020GL089894, doi: 10.1029/2020gl089894, 2020.
- Wik, M., Varner, R. K., Anthony, K. W., MacIntyre, S., and Bastviken, D.: Climate-sensitive northern lakes and ponds are critical components of methane release, *Nature Geoscience*, 9, 99-106, doi: 10.1038/ngeo2578, 2016.



935

Wille, C., Kutzbach, L., Sachs, T., Wagner, D., and Pfeiffer, E. M.: Methane emission from Siberian arctic polygonal tundra: eddy covariance measurements and modeling, *Global Change Biology*, 14, 1395-1408, doi: 10.1111/j.1365-2486.2008.01586.x, 2008.

940